A THESIS SUBMITTED TO
THE GRADUATE SCHOOL OF NATURAL AND APPLIED SCIENCES
OF ÇANKIRI KARATEKİN UNIVERSITY

PRODUCTION AND CHARACTERIZATON OF SnO_2:Cu/CdS FILMS FOR SOLAR CELL APPLICATIONS

IN PARTIAL FULFILLMENT OF THE REQUIREMENTS
FOR
THE DEGREE OF MASTER OF SCIENCE
IN
PHYSICS

BY

WALEED WASEA KHALAF ALKUBAISI

ÇANKIRI

2023

PRODUCTION AND CHARACTERIZATON OF SnO_2:Cu/CdS FILMS FOR SOLAR CELL APPLICATIONS

By Waleed WASEA KHALAF ALKUBAISI

June 2023

We certify that we have read this thesis and that in our opinion it is fully adequate, in scope and in quality, as a thesis for the degree of Master of Science

Advisor : Assoc. Prof. Dr. Olcay GENÇYILMAZ

Examining Committee Members:

Chairman : Assoc. Prof. Dr. Olcay GENÇYILMAZ
Department of Material and Material Processing Technologies
Çankırı Karatekin University

Member : Asst. Prof. Dr. İlker KARA
Department of Medical Services and Techniques
Çankırı Karatekin University

Member : Asst. Prof. Dr. Emrah SARICA
Department of Electric Electronic Engineering
Başkent University

Approved for the Graduate School of Natural and Applied Sciences

Prof. Dr. Hamit ALYAR
Director of Graduate School

I hereby declare that all information in this document has been obtained and presented in accordance with academic rules and ethical conduct. I also declare that, as required by these rules and conduct, I have fully cited and referenced all material and results that are not original to this work.

Waleed WASEA KHALAF ALKUBAISI

ABSTRACT

PRODUCTION AND CHARACTERIZATON OF SnO_2:Cu/CdS FILMS FOR SOLAR CELL APPLICATIONS

Waleed WASEA KHALAF ALKUBAISI

Master of Science in Physics

Advisor: Assoc. Prof. Dr. Olcay GENÇYILMAZ

June 2023

In this thesis, the production and characterization of SnO_2:Cu/CdS films which can be used for solar cell applications were carried out. SnO_2:Cu/CdS films were produced on glass substrates using chemical spraying technique. First of all, SnO_2, CdS, SnO_2:Cu films were produced as separate layers, and finally SnO_2:Cu/CdS heterojunction films were obtained. Structural, optical, electrical and surface properties of the produced films were investigated to determine the solar cell usage potential. It was determined that the films were polycrystalline in tetragonal structure. The preferred orientation of the CdS along (002) direction at $2\theta = 26.60^{o}$. The other peaks were detected at $2\theta = 44$ and 52^{o} which can be ascribed due to reflection from (110), and (112) planes of the hexagonal CdS structure. Atomic force microcope (AFM) results shows that the distribution of grains on the surface is almost uniform and homogeneous, and the film is without any cracks. The results showed that the average surface roughness of the SnO_2, CdS and SnO2:Cu/CdS films were 10.7 nm, 17.6 nm and 18.8 nm, respectively. A Scanning Electron Microscope (SEM) results shows that the surfaces of the prepared films have spherical particles, with a homogeneous distribution on the substrate, and there are no cracks on the surface of the film or large molecular agglomerations. Energy-dispersive X-ray spectroscopy (EDX) results shows that the the elements that formed the film (SnO_2) which are tin (Sn), chlorine (Cl), oxygen (O), and silicon (Si). UV-VIS spectrophotometer was used to determine the optical parameters of the films such as transmittance, absorption, band gap and refractive index. The average transmittance and band gap values of the films in the visible region were found to be ~70 % and 3.75 eV,

respectively. The calculated energy gap values for SnO_2, SnO_2:Cu, SnO_2:Cu/CdS, and CdS films were 3.90, 3.88, 3.75 and 2.28 eV respectively. With the temperature-dependent conductivity measurement, it was observed that the films had n-type conductivity. Besides, the resistivity values of the films decreased with Cu doping and the SnO_2:Cu/CdS films had low resistivity (3.25×10^{-3} Ωcm). The surface properties and elemental analyses of the films were examined using atomic force microscopy and scanning electron microscopy, and it was seen that they had a homogeneous surface morphology.

2023, 64 pages

Keywords: Solar cell, SnO_2:Cu/CdS films, Chemical spray technique, Resistivity, Activation energy

ÖZET

GÜNEŞ PİLİ UYGULAMALARI İÇİN SnO_2:Cu/CdS FİLMLERİNİN ÜRETİM VE KARAKTERİZAYONU

Waleed WASEA KHALAF ALKUBAISI

Fizik, Yüksek Lisans

Tez Danışmanı: Doç. Dr. Olcay GENÇYILMAZ

Haziran 2023

Bu tez çalışmasında güneş pili uygulamaları için SnO_2:Cu/CdS filmlerinin üretimi ve karakterizasyonu yapılmıştır. SnO_2:Cu/CdS filmleri cam tabanlar üzerine kimyasal püskürtme tekniği kullanılarak üretilmiştir. Öncelikle SnO_2, CdS, SnO_2:Cu filmleri ayrı ayrı katman olarak üretilmiş, son olarak da SnO_2:Cu/CdS heteroeklem yapılı filmler elde edilmiştir. Üretilen filmlerin güneş pili kullanım potansiyelini belirlemek için yapısal, optiksel, elektriksel ve yüzeysel özellikleri incelenmiştir. Filmlerin tetragonal yapıda polikristal olduğu tespit edilmiştir. Filmlerin geçirgenlik, soğurma, bant aralığı ve kırılma indisi gibi optik parametrelerinin belirlenmesinde UV-VIS spektrofotometre kullanılmıştır. Filmlerin görünür bölgede ortalama geçirgenlik ve bant aralığı değerleri de sırasıyla ~ % 70 ve 3,75 eV olarak bulunmuştur. Sıcaklığa bağlı iletkenlik ölçümü ile filmlerin n-tipi iletkenlik özellikte olduğu görülmüştür. Ayrıca, Cu katkısı ile filmlerin özdirenç değerleri azalmıştır ve SnO_2:Cu/CdS filmleri düşük özdirenç (3.25×10^{-3} Ωcm) değerine sahip olmuştur. Filmlerin yüzey özellikleri ve elemental analizleri atomik kuvvet mikroskobu ve taramalı elektron mikroskobu kullanılarak incelenmiş, homojen bir yüzey morfolojisine sahip olduğu görülmüştür. Enerji dağılımlı X-ışını spektroskopisi (EDX) sonuçları filmi oluşturan elementlerin (SnO2) kalay (Sn), klor (Cl), oksijen (O) ve silikon (Si) olduğunu gösterir. Filmlerin geçirgenlik, absorpsiyon, bant aralığı ve kırılma indeksi gibi optik parametrelerini belirlemek için UV-VIS spektrofotometre kullanılmıştır.Sıcaklığa bağlı iletkenlik ölçümü ile filmlerin n-tipi iletkenliğe sahip olduğu gözlemlendi. Ayrıca Cu katkılama ile filmlerin özdirenç değerleri düşmüş ve SnO2:Cu/CdS filmlerin özdirenci düşük (3.25×10-3 Ωcm) olmuştur. Filmlerin yüzey özellikleri ve elemental analizleri atomik kuvvet mikroskobu

ve taramalı elektron mikroskobu kullanılarak incelenmiş ve homojen bir yüzey morfolojisine sahip oldukları görülmüştür.

2023, 64 sayfa

Anahtar Kelimeler: Güneş pilleri, SnO_2:Cu/CdS filmleri, Kimyasal püskürtme tekniği, Özdirenç, Aktivasyon enejisi

PREFACE AND ACKNOWLEDGEMENTS

My first and big appreciation goes to my supervisor, Assoc. Prof. Dr. Olcay GENÇYILMAZ for her marvelous supervision, guidance and encouragement. Sincere gratitude is extended to her generous participation in guiding, constructive feedback, kind support, and advice during the search period. Many thanks to all of the members of staff in Faculty of Science for their kind support during my spell master's degree study. Also, I extend my thanks to all my colleagues at Çankırı university for their continuous encouragement and support. Last, but not least, my warm and heartfelt thanks go to my family for their tremendous support and hope they had given to me. Without that hope, this thesis would not have been possible. Thank you to everyone who helped me, even with a sincere word.

Waleed WASEA KHALAF ALKUBAISI
Çankırı-2023

CONTENTS

LIST OF SYMBOLS

A	Absorbance
I_A	Absorbed intensity
α	Absorption coefficient
Å	Angstrom
k_B	Boltzman constant
n	Carrier concentration
°C	Centigrade degree
N	Complex refractive index
σ	Conductivity
Cs	Crystal size
δ	Dislocation density
μ_e, μ_p	Electron and hall mobility
eV	Electron volt
E_g	Energy gap
d_{XRD}	Experimental distance
k_o	Extinction coefficient
β	Half peak width
V_H	Hall voltage
d_{hkl}	Interplaner distance
B_z	Magnetic field
S	Microstrain
μ	Mobility
M	Molar
nm	Nanometer
Ω.cm	Ohm.centimeter
h	Planck's constant
R	Reflectance
I_R	Reflected intensity
n_o	Refractive index
ρ	Resistivity
d_{CARD}	Standard distance
I_o	Standard intensity
T	Transmittance
I	Transmittance intensity
TCO	Transparent conductive oxides
V	Volt
ʎ	Wavelength

LIST OF ABBREVIATIONS

AFM	Atomic force microscope
EDS	Energy dispersive X-ray spectroscopy
FESEM	Field emission scanning electron microscope
UV- VIS	Ultraviolet-visible
XRD	X-ray diffraction

LIST OF FIGURES

LIST OF TABLES

1. INTRODUCTION

One of the most promising solutions for the planet's energy future is photovoltaics. Photovoltaic energy comes from the conversion of sunlight into electricity. It is ensured through semiconductor materials, such as transparent conductive oxides (TCO). From a technological point of view, their field of application is vast; they are found in various areas such as Electronics, optoelectronics, photothermal conversion, photovoltaic conversion, etc (King and Veal 2011).

Semiconductor materials are insulators at absolute zero degrees. In other words, there are no free charge carriers in semiconductors at this temperature. In order for the electrons to pass from the valence band to the conduction band and become free, they must receive energy from the outside. This amount of energy must be equal or higher than as the fobidden band gap energy in semiconductors. The forbidden gap is the term used to describe the difference between the valence band and the conduction band (Al-Hakim and Hussein 1980). Therefore, both electrons and holes can be conducted in semiconductors (Smith 1987). Semiconductors are classified according to their crystalline structure as crystalline or amorphous semiconductors. Where crystalline semiconductors are divided into single crystalline, and polycrystalline (Al-Jubouri and Hayati 1985). The branch of thin film physics is one of the most important branches of solid-matter physics (Hass *et al.* 2013). It has attracted great interest from researchers over the past decades, and films have been developed through various deposition processes to obtain optical, electrical, and synthetic properties used in various applications (Chopra 1969). The different many types of research were conducted in this field by many scientists, we mention of which:

In the year 1852, two scientists (Bunsen and Crove) prepared a thin metal layer using the method of chemical reactions (Eckertova 1977).

In the year 1857, the scientist (Faradi) prepared a thin layer using vacuum evaporation (Eckertova 1977).

In the year 1887, the scientist (Kentt) prepared a thin layer using the method of evaporation in a vacuum (Leaver 1971).

In 1879, the scientist E. H. Hall determined the density of charge carriers of different types, which was named after him the Hall effect, and this discovery is the actual emergence of semiconductors. Then followed the discovery of the world J. J. Thomson of the electron in 1897, which helped in the development of the theoretical description of electrical conductivity, three years later came the discovery of the scientist P. Drude to provide a model describing the electrical and thermal conductivity of solid materials (Grahn 2001).

Transparent Conductive Oxides (TCO), it was discovered in 1907 by the German scientist (Baedeker 1907) who was able to prepare a thin layer of cadmium oxide (CdO), which is characterized by its electrical conductivity and its transparency to visible light. Although CdS is not widely used today due to toxicity concerns, it is still of theoretical interest due to the high electron mobility due to the low effective electron mass (Jones *et al.* 2009).

In 1937, tin oxide (SnO_2) was deposited by the method of post-oxidation of evaporated thin films (Mattox and Mattox 2007). However, technological progress in transparent conductive oxides did not appear until after 1940, when potential applications became in the industry (Retnasamy *et al.* 2014).

Then, studies in this field followed, where many transparent conductive oxides were discovered, such as indium oxide (In_2O_3), zinc oxide (ZnO), tin oxide (SnO_2), titanium oxide (TiO_2) ... etc. The most common is indium tin oxide (ITO), but due to its high cost, it is replaced by doping oxides with metal elements such as zinc oxide doped with aluminum (ZnO: Al), tin oxide doped with various impurities such as fluorine, cadmium and copper (SnO_2:Cu, SnO_2, Cd, SnO_2:F) etc. In recent years, tin oxide has received more attention because it can overcome the problem of the high cost of indium (Hernández 2021).

1.1 Transparent Conductive Oxides (TCO)

Transparent conductive oxides (TCO) are compounds composed of metal combined with oxygen, and they may be binary or ternary compounds containing one or two metallic elements. TCO has two main advantages. These are high electrical conductivity and high optical transmittance in the visible part of electromagnetic spectrum. Metal oxides, such as In_2O_3, SnO_2, ZnO, etc., are considered electrical insulators, but due to a large number of defects (oxygen vacancies), they conduct electricity. Conductivity can be adjusted by controlling the addition of impurities. Hence, positively charged (p-type) and negatively charged (n-type) semiconductors can be produced. Therefore, it has opened technological applications for a wide range of photovoltaic circuits as well as other applications in various fields. The electrical and optical properties of transparent conductive oxide films are affected by several factors such as temperature, thickness, and the type of technology used to prepare the films (Boufaa 2012). Transparent conductive oxides have the behavior of semiconductors and have several advantages (Abd 2012).

- It has a high sensitivity when it contains impurities that lead to an increase in its conductivity and the appearance of one type of charge carrier.

- When the temperature increases, its electrical conductivity increases and it behaves like an insulator when the temperature decreases.

- It has high transmittance in the optical wavelengths (400-800 nm) of the electromagnetic spectrum.

1.2 Properties and Applications of Tin Oxide (SnO_2) Films

Transparent conductive oxides are used in many applications, and tin dioxide (SnO_2) is one of the low-cost materials compared to other transparent conductive oxides. It is thermally stable, and chemically stable when dealing with acids and bases. It is also

considered a material with good mechanical properties, so it has wide applications, such as (Dekkers 2007):

- Solar cell, as a conductive window layer
- Heat-reflecting windows (buildings, ovens etc.)
- Flat screens
- Thermal insulating glass
- Mirrors and electrochemical cell
- Optoelectronics (LEDs.)
- Touch control devices
- Gas sensors

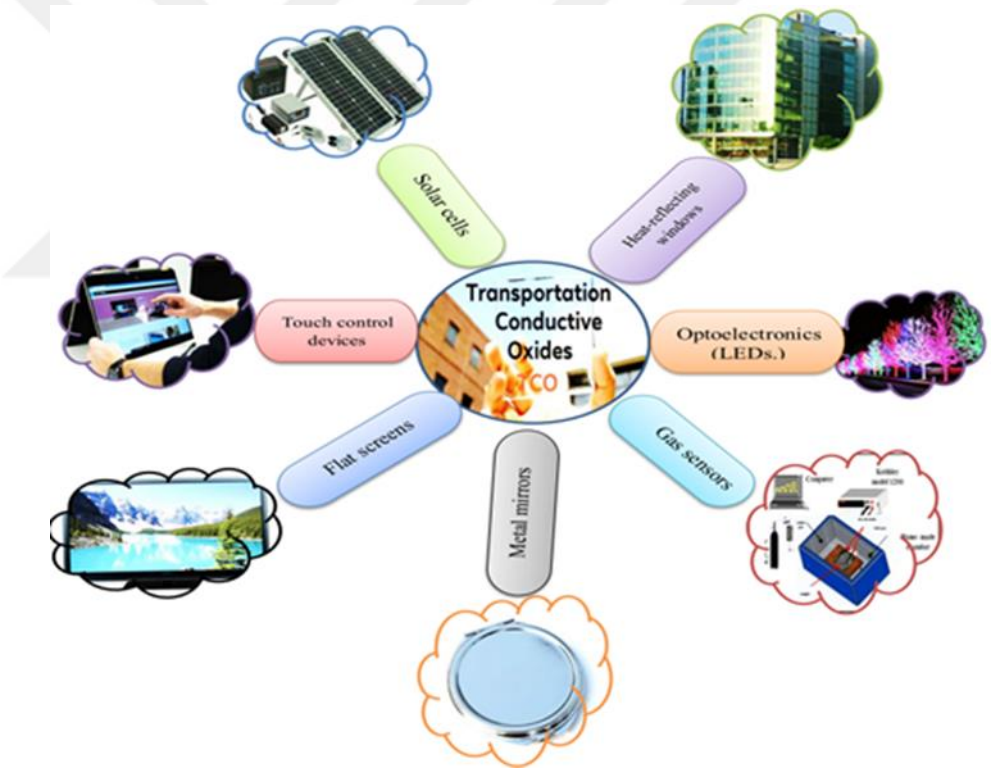

Figure 1.1 The applications of TCOs (Dekkers 2007)

The structure of tin dioxide is of the rutile type; its space group is P4/mm. The unit cell is generally quadratic (tetragonal) (a = b = 0.475 nm and c=0.318 m) and contains six atoms: two tin atoms and four oxygen atoms. Each tin atom is the center of an almost

regular octahedron formed by six oxygen atoms, while each oxygen atom is surrounded by three tin atoms located at the vertices of an isosceles triangle. The ionic radii of the Sn^{4+} cation and the O^{-2} anion have values of 0.071 and 0.14 nm, respectively (Yahiaoui 2014 and Maache 2014). A schematic representation of a unit cell of tin dioxide is shown in Figure 1.1 and Figure 1.2.

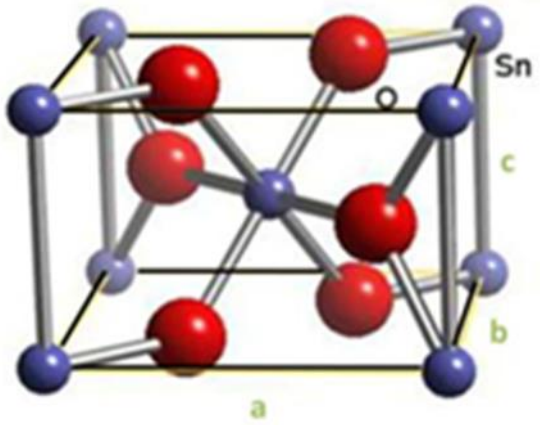

Figure 1.2 Unit cell of SnO_2 (rutile structure) (Yahiaoui 2014)

SnO_2 films have a wide direct bandgap (3.6 - 4.2 eV) and it varies with different deposition methods. The concept of a direct or indirect energy gap (also known as a forbidden band) is related to the position of the maximum values of the valence band and the minimum values of the conduction band. Figure 1.3 represents the energies as a function of the wave vector (**k**). If both the valence band and the conduction band correspond to the same wave vector (**k**), then the transition of electrons is perpendicular and is called direct transmission. But if the minimum values of the conduction band shift so that they do not correspond to the maximum values of the valence band, it is called indirect transition (Robertson 1979).

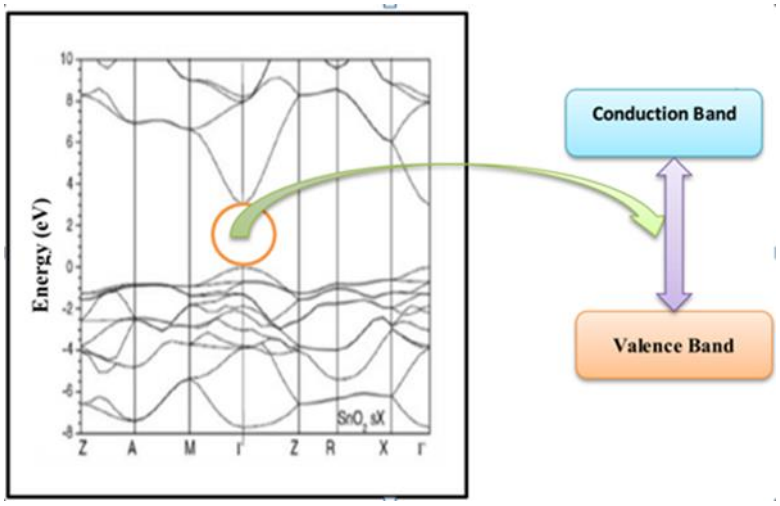

Figure 1.3 The optical energy gap of tin oxide (SnO_2) (Robertson 1979)

The optical properties of tin oxide depend on the interaction of photons of electromagnetic waves and electrons in a semiconductor (Figure 1.3). The electrons of the material absorb the energy of the incident photons. If the energy of the photon is equal to or greater than the energy of the gap, then the electrons transition from the valence band to the conduction band. Tin oxide has an energy bandgap (3.6 eV) in the form of thin films having high transmittance within the visible region of the electromagnetic spectrum (400-800 nm) as shown in Figure 1.4. Table 1.1 summarizes the basic properties of tin oxide (Boufaa 2012).

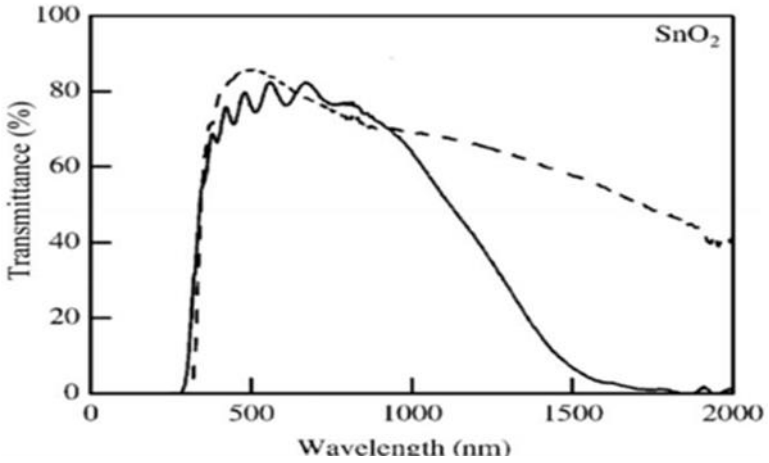

Figure 1.4 Transmittance of tin oxide (SnO_2) (Robertson 1979)

Table 1.1 Physical and chemical properties of tin oxide (SnO_2)

PROPERTIES	SPECIFICATION
Chemical formula	SnO_2
Molecular weight	150.69 g/ mole
Band gap	3.6 eV at room temperature
Color	White or gray
Melting temperature	1500-1630 ºC
Boiling point	1800- 1900 ºC
Density	6.90 g/cm^3
Crystal structure	Tetragonal
Molar mass	150.69 g/mol

Stoichiometric Tin oxide (SnO_2) is an insulating material at room temperature, but it is well known point defects such as oxygen vacancies (V_O) or tin interstitials (Sn_i) led to have n-type conductivity at room temperature. Additionally, electrical properties can be further enhanced by doping with elements such as copper, aluminum, fluorine, antimony, indium, and zinc. The doping increases the number of charge carriers (electrons) and then increases its electrical conductivity (i. e. The resistivity of this n-type semiconductor decreases) (Ynineb 2010, Kasap 2002).

1.3 Properties of Cu Element

Copper (Cu) is one of the most important chemical and transitional elements in nature and is often found in nature in the form of divalent Copper (Cu^{+2}). It crystallizes in a face-centered cubic structure. Table 1.2 summarizes the most important physical and chemical properties of Copper (Hamrouni and Balila 2017, Thompson 1964, Hernández-Arteaga *et al.* 2021).

Table 1.2 Physical and chemical properties of Copper (Cu)

PROPERTIES	SPECIFICATION
Chemical formula	Cu
Molecular weight	63.546 g/mole
Melting temperature	1083.45 ºC
Boiling point	2567 ºC
Color	Reddish brown
Density	8.96 g/cm^3
Crystal structure	Face-Centered Cube
Atomic number	29
Specific resistance	1.77×10^{-8} Ωm

1.4 Properties of Cadmium Sulfide (CdS)

Cadmium sulfide (CdS) is a semiconductor compound and is formed from group II-VI elements of the periodic table. The crystal structure of cadmium sulfide is a hexagonal and zinc blend as shown in Figure 1.5. CdS crystal has a yellow-orange color. The unit cell of CdS is a face-centered cubic (fcc) and hexagonal close-packed (hcp) structure Also, the bond between sulfur and cadmium ions is a covalent bond due to the sharing of two electrons between the cadmium atom and the sulfur atom.

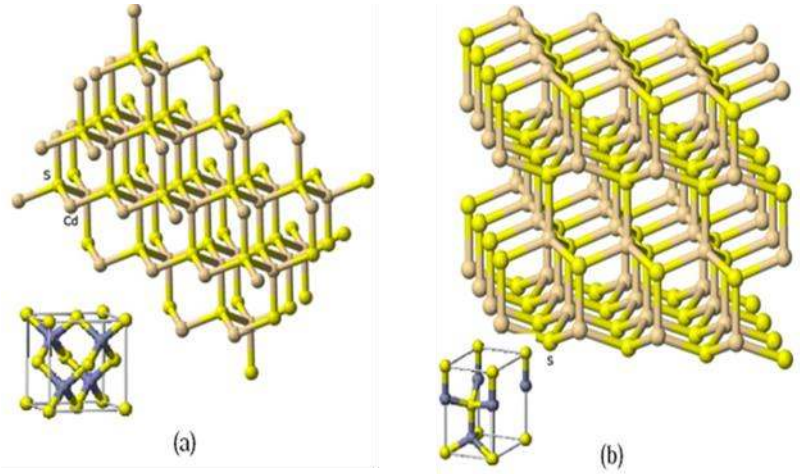

Figure 1.5 Crystal structures of CdS (a) zincblende and (b) wurtzite (Ismail 2008)

Cadmium sulfide has a direct energy gap of 2.4 eV at 300 K. Therefore, the cut-off wavelength at 2.4 eV is 520 nm in the green region of the visible spectrum. From this, we conclude that the absorption of the film is at short wavelengths, while the film has more transmittance at long wavelengths (Kwok 1995, Jassem 2004, Badeker 1907). Some physical and chemical properties are summarized in Table 1.3.

Table 1.3 Physical and chemical properties of CdS

PROPERTIES	**SPECIFICATION**
Chemical formula	CdS
Crystal structure	Hexagonal, Cubic
Molecular Weight	144.46 g/ mole
Band Gap	2.42 eV at RT
Color	Yellow
Melting temperature	2023 ºC
Density	8.96 g/cm^3
The refractive Index	2.3- 2.6
Dielectric constant	8.64

1.5 Aim of the Research

CdTe/CdS is one of the commercial thin film solar cells, it is not widely used. These solar cells have a stable structure and are economical. Since the front contact material in the solar cell is expected to be low resistivity and high transmittance, transparent conductive oxide materials (TCO) are used in this part. However, after this layer, other layers with which sunlight will interact must be.

In recent years, research and development of double-layer films have been focused on increasing this stability. This thesis aims to produce double-layered SnO_2:Cu/CdS heterostructure films by optimizing Cu-doped SnO_2 films as an alternative to the most widely used TCO films such as ZnO. In addition, by examining some physical

properties of these films, it is to determine their potential for use in different application areas.

For this reason, in this thesis, we focused on the production and physical properties of SnO_2:Cu/CdS heterostructure films that can be used in solar cells with the chemical spray technique, which is a practical and economical technique.

2. LITERARURE REVIEW

There are many research papers that have included good review articles on the properties of pure or doped tin dioxide. But few studies included doping the tin dioxide with the precipitated copper. In this paragraph, we will review the studies related to our current research.

Pawan both theoretically and experimentally, the structural and optical changes in the SnO_2 system brought about by the introduction of Cu in a SnO_2 system (Chetri *et al.* 2013). The results show that The introduction of Cu in the SnO_2 system brings distortion which is corroborated by the variation in the corresponding bond lengths. XRD and Raman measurement shows that the doping of Cu removes Sn^{2+} from the system. The increase in Urbach energy with Cu doping indicates distortion in the system.

Kumar (2014) shows that the structure is very stable and has a very narrow interface. Since these two layers are widely used in thin film solar cells, the stability of the CdS/SnO_2 interface is very important (Kumar 2014).

Liu *et al.* (2015) found that SnO_2 nanoparticles can be tightly anchored on the surface of CdS NRs, and the thickness of SnO_2 shells can be conveniently adjusted by simply changing the additional amount of SnO_2 quantum (Liu *et al.* 2015).

Orimi and Maghouli (2016) studied the optical properties of SnO_2 nanostructured films at different temperatures using the thermochemical decomposition technique. XRD results showed that the crystal size increases and the transmittance decrease with the increase in the annealing temperature. As well as the energy gap gradually decreases with increasing annealing temperature (Orimi and Maghouli 2016).

Reddy *et al.* (2017) synthesized CdS, SnO_2, and CdS/SnO_2 hybrid photocatalyst nanostructure. The band gap energies calculated are 3.30, 2.15, and 2.99 eV for pristine SnO_2, CdS, and the CdS/ SnO_2 hybrid photocatalyst, respectively (Reddy *et al.* 2017).

The crystal structure of the prepared photocatalysts is confirmed as hexagonal and tetragonal rutile structures of CdS and SnO_2 respectively. Also, the results show that the presence of SnO_2 nanoparticles reduced the aggregation of CdS nanoparticles, thereby increasing the surface area.

Khlayboonme and Thowladda (2018) synthesized thin films of un-doped and Cu-doped tin oxide. XRD patterns of all films exhibited rutile-phase SnO_2 (Khlayboonme and Thowladda 2018). The Cu doping content decreased the optical bandgap from 4.36 eV for undoped SnO_2 to 4.28 eV for 3 % Cu-doped SnO_2. The further Cu doping content increased the bandgap energy to 4.32 eV. The resistivity was increased for doping of Cu 1 % but it was decreased with further increases in Cu-doping contents.

Zhou *et al.* (2019) found that the prepared SnO_2 (TiO_2)/CdS heterostructure showed much higher photocatalytic activities for the degradation of the methyl orange (MO) under visible light irradiation in comparison with individual SnO_2 (TiO_2) film photocatalyst (Zhou *et al.* 2019).

Dolaiet *et al.* (2019) fabricated Glass/F:SnO_2/CdS/CuO/Ag heterostructure using direct current (d.c) magnetron sputtering and thermal evaporation technique (Dolaiet *et al.* 2019). The above heterojunction structure shows the efficiency ~2.1 %. The open-circuit voltage of the cells was ~0.462 V. The efficiency values obtained here are the highest compared to those reported so far for this glass/F: SnO_2/CdS/CuO/Ag structure.

Mohammad and Mohammed (2020) fabricated SnO_2 and SnO_2/CdS layers by solution process using a suspension including CdS nanoparticles synthesized via a simple solution route (Mohammad and Mohammed 2020). The results show that a thin interface layer of CdS nanoparticles on top of the SnO_2 layer consistently improves the electron transport properties of the SnO_2 layer. CdS interface layer can act as an intermediate step to facilitate electron transfer from the perovskite layer to SnO_2.

El-Katori *et al.* (2020) synthesized CdS/SnO2 heterostructure without any distortion in crystalline parameters (El-Katori *et al.* 2020). CdS quantum dots of size 9 nm, surface

area 26.5 m^2/g, and wide mesoporous size (pore radius = 119.2 Å) were incorporated homogeneously on the surface of SnO_2 forming an efficient heterojunction that cause a remarkable reduction in the band gap energy of SnO_2 from 3.52 to 2.53 eV.

Hasan *et al.* (2020) fabricated tin oxide (SnO_2) thin film with a thickness of 300 nm on a glass substrate XRD patterns revealed Al and Cu doped SnO_2 thin film proved it as a polycrystalline with cubic phase and variable miller indices at peak XRD intensity (Hasan *et al.* 2020). Transmittance in the near-infrared region for the undoped film is approximately 70 % and for both Al and Cu doped films it is below 35 %. Reflectance gets higher as the percentage of Al and Cu doping increases; the energy bandgap falls from 3.72 eV to 3.42 eV and both the refractive index and dielectric constant get higher as the percentage of Al and Cu doping enhances.

Su *et al.* (2021) developed a simple method to synthesize SnO_2 colloidal as a precursor solution at room temperature (Su *et al.* 2021). Also, prepared SnO_2/CdS double electron transport (ETL) layer was prepared by combining SnO2 and CdS layers. Experimental analyses revealed that the introduction of SnO_2 ETL enhanced the grain size of Sb_2S_3 films and passivated interfacial defects thus enhancing device efficiency.

Sharma *et al.* (2021) reported SnO_2-CdS nanocomposites synthesized using a two-step solution route on a cellulose acetate flexible substrate using a spin coating (Sharma *et al.* 2021). Shift in X-ray diffraction confirms the formation of nanocomposites due to tensile strain. The roughness of SnO_2-CdS nanocomposites decreases as compared with pure SnO_2. Optical transmittance shows an additional band at 500 nm confirming the formation of nanocomposites.

Abbas *et al.* (2021) report various properties of four Cu-doped SnO_2 thin films on a glass substrate at a temperature of 80 ºC via the standard chemical bath deposition method (Abbas *et al.* 2021). The XRD analyses of the studied CuSnO-TFs showed their body-centered tetragonal structures in a rutile phase with high purity and good polycrystallinity. The average crystallite size was increased from 17.6 to 34.52 nm with

the increase of Cu contents from 0 to 3 %, respectively. Both visible transmittance and optical band gap energies of the films were decreased with the increase of Cu levels.

Shaker *et al.* (2022) synthesized pure SnO*2* nanoparticles doped with Cu by a chemical precipitation method (Shaker *et al.* 2022). The crystal (tetragonal) of SnO*2* does not change with the introduction of Cu and the crystal size varies with the change of Cu doping. The results of the AFM show that the grain size within the nanoscale is spherical in shape. The results of the AFM show that the grain size within the nanoscale is spherical in shape. The energy gap increases with increasing doping.

3. MATERIALS AND METHODS

This section contains theoretical information about the production and characterization techniques used in the thesis.

3.1 The Growth Mechanisms and Some Physical Properties of Thin Film

There are many physical and chemical methods that were used to prepare thin films (Eckertová 1977). The preparation methods can be divided into two basic categories as in Figure 3.1.

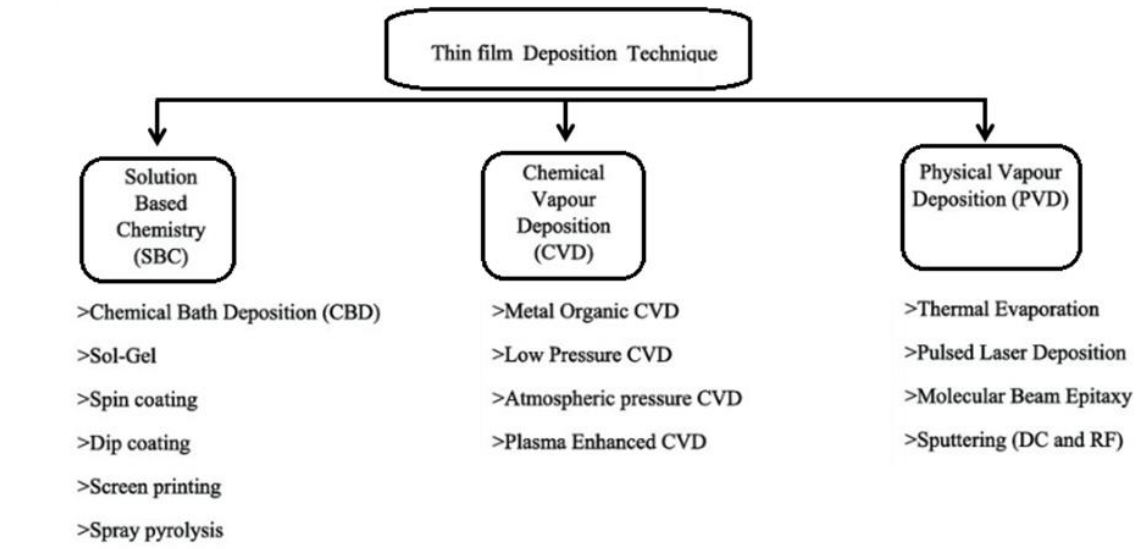

Figure 3.1 Methods of thin film deposition

In physical methods (physical vapor deposition), the material is obtained by evaporation or bombardment by electrons, photons, or ions, which depends on physical processes such as thermal evaporation. The substance transformed into vapor will condense on the surface of the substrate. Thus, there are no chemical reactions that occur in this process. As for the chemical methods, the chemical reaction consisting of a mixture of materials deposited on the substrate will produce a thin film with the required composition while the elements of secondary reactors are eliminated. The researchers have worked to

develop modern technologies and employ them in practical applications by controlling deposition conditions.

Among these techniques, the chemical spraying technique (CSPT) draws attention as it is a practical and economical technique. This technique is one of the chemical methods in which the solution is sprayed onto heated glass substrates at a fixed temperature. The chemical reaction takes place on the surface of the substrate. This technique depends on the following parameters (Khaled 2012):

- Substrate temperature
- Quality of the substrate
- The size of the spray droplets
- The distance between the substrate and the nozzle
- Deposition rate
- Type of carrier gas and its pressure

Chemical Spray Pyrolysis technique is widely used by researchers due to the following advantages:

- Cheap and simple
- Used for large areas
- Deposition parameters can be easily controlled
- In this technique it is possible to prepare films for materials that are used in high-temperature applications that are difficult to prepare with other techniques.

The main parts of the chemical spray pyrolysis system (Saleh and Labihat 2018):

Nozzle: It is a device with three apertures. The aperture is connected to a tube at the end of which is a beaker (100 ml) containing the solution, and the second tube passes through which compressed air from the air compressor so that both the solution and the compressed air come out from the third aperture, which is called the main aperture.

Also, another advantage of the nozzle is that it can control the speed of the solution flow. A photograph of a commonly used nozzle is given in Figure 3.2.

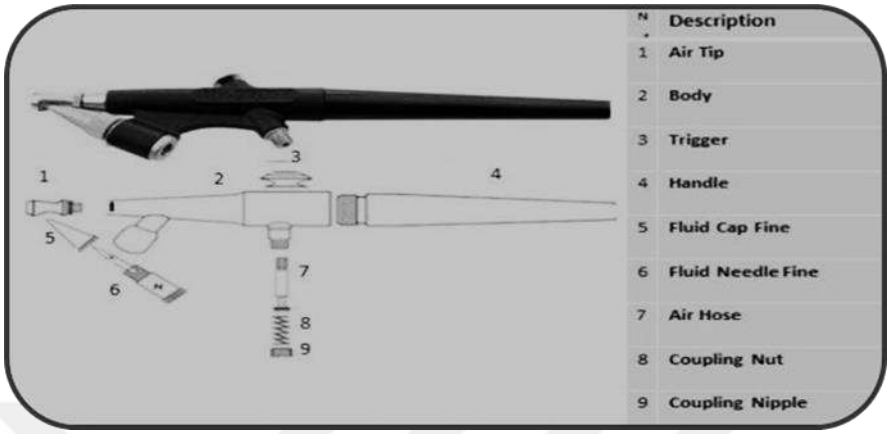

Figure 3.2 Schematic diagram of the nozzle (Mahdi 2016)

Electric heater: The electric heater is used to control the temperature of the glass substrate. The deposition temperature causes a change in the crystalline structure of the material and this leads to a change in its physical properties. The electric heater is connected to a controller.

Air compressor: It contains a regulator through which the air pressure is controlled and directed towards the spray device, to ensure that the solution reaches to the substrate in the form of a fine drop.

Digital multimeter: It is a device used to know the temperature of the glass substrate placed on the electric heater. Also, it is possible to control the spray rate and the stopping time through it.

Accordingly, the solution droplets that start to flow from the spray head have quite large dimensions in the 1st case and the heat received by the droplet from the environment is not enough for it to evaporate until it reaches the bottom. Thus, when the droplet hits the bottom, it evaporates leaving a dry precipitate, the temperature of the bottom drops, and a bad film is formed. In case 2, the droplets are smaller in size than in case 1, and some of the droplets evaporate and condense. The droplets dry before reaching the

bottom and hit the surface. In this case, cracks, holes, or spalling may appear on the surface. Case 3 is the ideal transport case, which indicates that the solution droplets have completely evaporated when they approach the bottom. In this case, the droplets are even smaller than the droplets in the 1st and 2nd cases and evaporate as soon as they reach the surface. Thus, they create a heterogeneous reaction and adhere to the surface. This heterogeneous reaction includes physical and chemical events such as settlement and diffusion within the lattice. In case 4, the droplets are at their smallest size. In this case, the droplets evaporate before reaching the bottom and create a homogeneous reaction in the vapor phase. The molecules attached to the base are in powder form and a good film formation does not occur Figure 3.3 and Figure 3.4 (Gençyılmaz 2013).

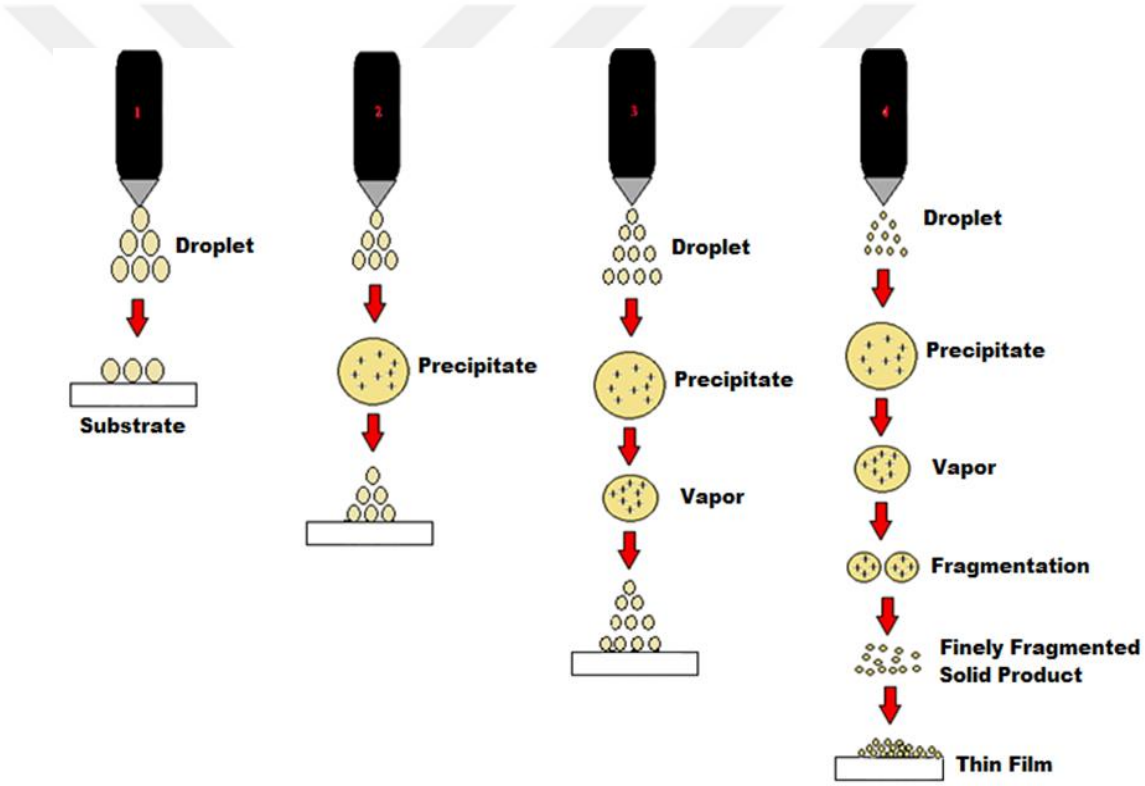

Figure 3.3 Effect of droplet size on the mechanism of thin film formation (Gençyılmaz 2013)

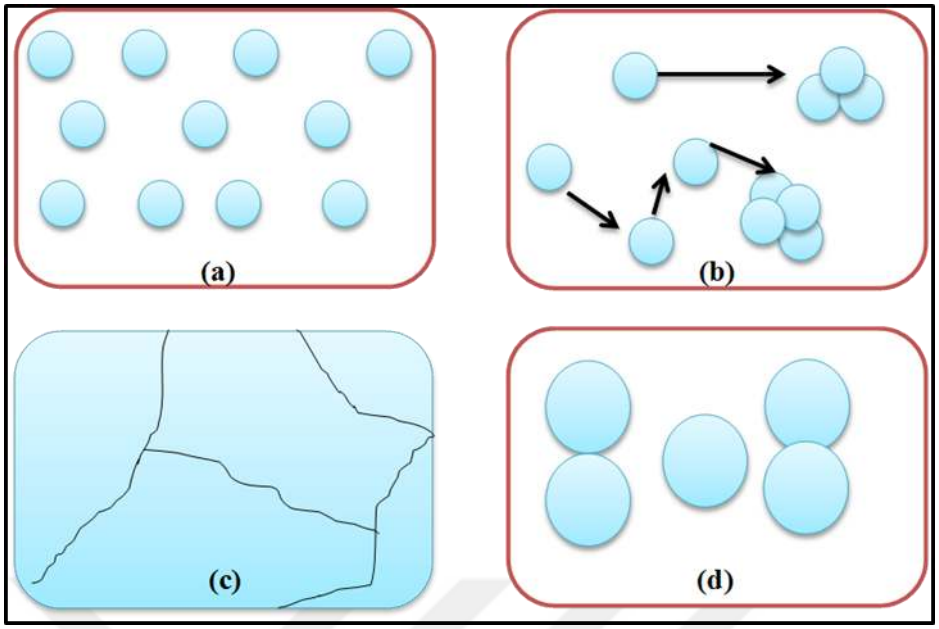

Figure 3.4 Mechanisms of film growth (a) nucleation (b) aggregation (c) and (d) croissance

The structural properties are very important to determine the crystal structure of films. X-rays are used to determine the nature of the crystal structure, crystal phases, and the preferred orientations of the films (Al-Dulaimi 2011). When X-rays (0.01- 10 nm) incident the film, part of these rays will be reflected by the atomic levels of the crystals in certain directions with different intensities. The reflected waves (of the same phase) from these planes interfere with each other constructively, and this interference is obeyed by the condition of Bragg's law, which is given by the following relationship (Hafdallah 2007). Equation (3.1):

$$2\,(d_{hkl})\sin\theta = n\lambda \qquad (3.1)$$

where n is the order of reflection, n=1, 2, ...etc., λ is (X-ray wavelength, λ =1.5401 Å), d is the interplaner distance, θ is Bragg's angle.

The crystallite size (C_s) of crystalline material has an important role in determining the properties of the material which can be found using Scherer's formula in Equation (3.2) (Cullity 1978).

$$D = \frac{k\lambda}{\beta \cos\theta} \tag{3.2}$$

where k is shape factor, β is full width at half maximum (FWHM).

The strain (ε), Dislocation density (δ), microstrain (S), number of layers (N_L), and number of crystallites per unit area (N_0) of films can be calculated from the following relation (Ivashchenko and Kerner 2003, Paufler 1980, Wang 2009 and Šutta and Jackuliak 1998). Equation (3.3), Equation (3.4), Equation (3.5), Equation (3.6):

$$\varepsilon = \frac{\beta \cos\theta}{4} \tag{3.3}$$

$$\delta = \frac{1}{(Cs)^2} \frac{lines}{(nm)^2} \tag{3.4}$$

$$S = \frac{|d_{XRD} - d_{CART}|}{d_{CARD}} \tag{3.5}$$

$$N_0 = \frac{t}{(D)^3} \frac{1}{(nm)^3} \tag{3.6}$$

where d_{XRD} is the experimental distance, d_{card} is the standard distance, t is film thickness in (nm). Various techniques are used to study the surface properties of thin films. Among these techniques, atomic force microscopy (AFM) is used to determine the surface topography, while scanning electron microscopy is used to determine the surface morphology. Atomic force microscopy is used to analyze the morphology of the surfaces of materials to interpret the properties and behavior of that material to use in different applications. The purpose of the study of morphology is to determine how atoms are distributed and arranged on the surface. The atomic force microscope, Figure 3.5 consists of a Cantilever at the end of which there is a probe consisting of a sharp tip used to scan the surface of the sample (Adams 2007, Rengaraj 2011, Jagtap and Ambre 2006).

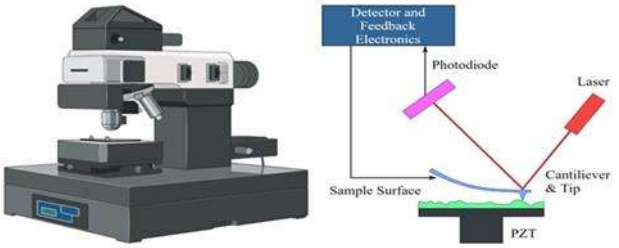

Figure 3.5 Schematic diagram of the atomic force microscope (Jagtap and Ambre 2006)

SEM uses high-energy electron radiation to obtain high-resolution images of the sample surface. Electrons are emitted from a cathode made of tungsten designed for high temperatures. The interactions between the electrons and atoms of the material deposited on the substrate give information about the topography of the sample surface, as well as the distribution and size of the particles. The SEM device is equipped with an EDX analysis unit, which is used for qualitative and quantitative analysis of the elemental compositions of the samples (Figure 3.6) (Postek 1980).

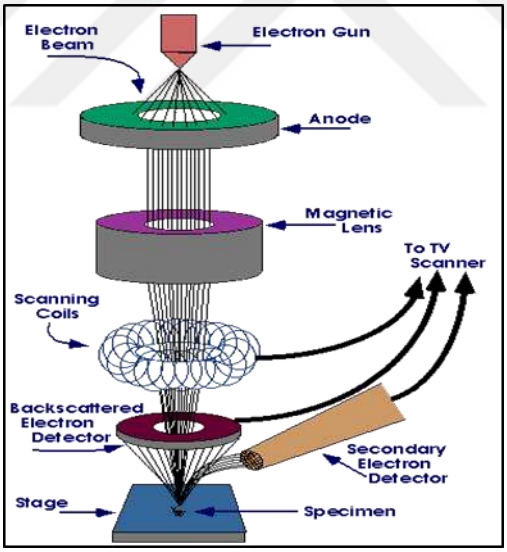

Figure 3.6 The schematic diagram of field emission scaning electron microscopy (FESEM) (Postek 1980)

Another feature that needs to be analyzed while determining the potential for the use of thin films in optoelectronic devices is the optical properties of the films. The optical properties of semiconductors play an important role for them, as they give us information about the electronic transitions from the valence band (*V.B*) to the

conduction band (*C.B*). The basic absorption region, which gives the value of the energy gap (E_g), is formed as a result of the absorption of light. The optical properties were studied using UV-VIS Spectrophotometer for the range (300 - 1100 nm). The optical studies include transmittance (*T*), absorbance (*A*), and reflectance (*R*), as well as optical constants, which include refractive index (*n*) and attenuation coefficient (*k*). All of these properties depend on the structure of the crystalline film, the thickness of the film, the type of film material as well as on the substrate temperature, and the other conditions of preparation of the thin films. Any change in one of these parameters could lead to a deviation of the absorption edge to higher or lower energies (Seeger 1995, Bass *et al.* 1995).

The part of the spectrum in the region of the absorption edge gives much useful information about the material under investigation (Tauc 1974), such as the type of transition, band gap energy (*Eg*), transmittance, and other optical properties of semiconductors (Ray 1969). When an electromagnetic wave interacts with valence electrons, electrons will move to a conduction band across the forbidden energy gap. Absorption appears when the photon energy is absorbed by an electron that equals or is greater than the forbidden energy gap. The electronic transitions between the valence band and the conduction band start at the absorption edge. These transitions are divided into direct and indirect transitions (Mott 1979, Neaman 1992).

This transition takes place in crystalline, polycrystalline semiconductors and amorf material (Seeger 1995). It can be defined as a direct vertical transition of an electron in the space of the wave vector of the valence band to the conduction band of wave vector values ($\Delta \boldsymbol{k} = 0$) where the conservation laws of momentum and energy are achieved (Mott and Davis 1979). The absorption coefficient is given by the Tauc relation (Pankove 1971), as follows in Equation (3.7):

$$\alpha h\nu = A_o \left(h\nu - E_g\right)^n \qquad (3.7)$$

where E_g is optical energy gap, α is absorption coefficient, *n* is constant depends on the transition from VB (Valence Band) to CB (Conduction Band).

Direct band transitions are divided into two, allowed direct transition and forbidden indirect transition. Allowed direct transition occurs directly with the shortest vertical distance from the top of the VB to the bottom of the CB and the same values of the wave vector (***k***) (i.e. momentum is conserved), as shown in Figure 3.7 (a). The value of (*n*) in Equation 3.7 is equal to 0.5. The forbidden indirect transition occurs vertically from the areas adjacent to the highest point in the VB to the points adjacent to the lowest point in the CB, as shown in Figure 3.7, n = 3/2) in Equation 3.8.

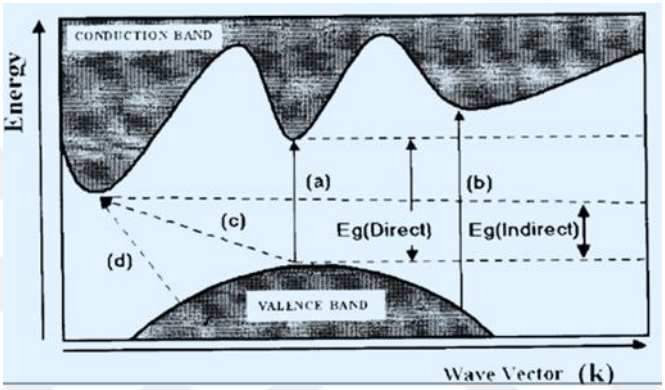

Figure 3.7 Electronic transitions (a) allowed direct transition, (b) forbidden direct transition, (c) allowed indirect transition and (d) forbidden indirect transition (Sze 1986)

Transmittance (*T*): the ratio between the intensity of transmitted light (I_T) to the intensity of incident light (I_o), and it is given by the following Equation (Sze 1986):

$$T = \frac{I_T}{I_\circ} \tag{3.8}$$

The transmittance depends on several factors such as film thickness, the temperature of the substrate, and doping.

Absorbance (*A*): The absorbance is defined as the ratio between the intensity of the absorbed ray (I_A) to the intensity of the incident ray (I_o), and it represents the value of the decrease in the energy of electromagnetic radiation in the material, and that the

absorbance depends on the thickness and nature of the material, and it can be calculated using the following in Equation (3.9):

$$A = \frac{I_A}{I_\circ} \tag{3.9}$$

Reflectance (*R*): The absorbance is defined as the ratio between the intensity of the reflected ray (I_R) to the intensity of the incident ray (I_o), and it can be calculated using the following in Equation (3.10):

$$R = \frac{I_R}{I_\circ} \tag{3.10}$$

Absorption represents the reduction that takes place in the energy of electromagnetic radiation when entering a specified medium (Chopra 2005). Accordingly, the absorption coefficient is defined as the reduction ratio in the energy of the incident ray ($I_{inc.}$) as a function of distance inside the medium. So when the light of intensity (I_0) incidents on a film of a thickness (t), then the intensity of transmittance ray (I) is given by (Pankove 1971) in Equation (3.11):

$$I = I_\circ \, e^{-\alpha t} \tag{3.11}$$

This Equation was achieved by Bouger in 1739 then approved by Lambert. It can also be written as follows in Equation (3.12), and Equation (3.13):

$$\ln \frac{I}{I_\circ} = -\alpha t \tag{3.12}$$

$$\alpha t = 2.303 \log \frac{I_\circ}{I} \tag{3.13}$$

Since the amount ($\log \frac{I_\circ}{I}$) represents the absorbance (A) of the film, so the in Equation (3.17) can be re-written as follows Equation (3.14):

$$\alpha = 2.303 \frac{A}{t} \tag{3.14}$$

The energy gap (E_g) is defined as the energy required for transferring electrons from the highest point in the valence band to the bottom point of the conduction band. It is called the forbidden region because its energy levels are free of charge carriers (electrons). In pure semiconductors, no electrons exist in the forbidden region, while in doped semiconductors the electrons are present for a very short time. The energy gap is an important optical parameter, many optical devices depend on the value of the optical energy gap such as solar cells, etc. Figure 3.8 shows the optical energy gap of tin oxide. The absorption coefficient is related to the optical energy gap by the following Tauc relationship (Runyan 1975) Equation (3.15):

$$(\alpha h\nu)^2 = \beta(h\nu - E_g) \tag{3.15}$$

where β is a constant that depends on the type of material, $h\nu$ is photon energy in (eV), E_g is optical power gap in (eV), α is absorption coefficient.

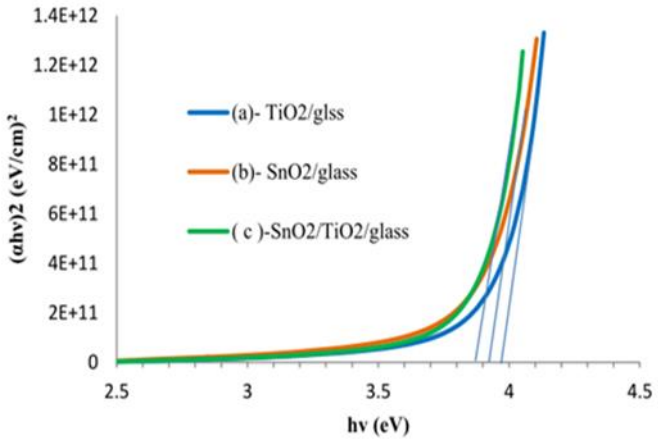

Figure 3.8 The energy gap of the SnO_2 film (Mohammad and Mohammed 2020)

The refractive index (n) of a material is the key parameter for device design. In semiconductors, the evaluation of the refractive index is of considerable importance for applications in integrated optics. The refractive index has represented the ratio between

the velocities of the wave in free space (vacuum) to its velocity in the medium (Millaman 1979, Ravindra 2007) Equation (3.16):

$$n_\circ = \frac{c'}{v} = n_\circ - ik_\circ \tag{3.16}$$

where c' is the speed of light in a vacuum, and v is the speed of light in the medium. The refractive index depends on several factors such as the type of materials and crystal structure. The refractive index is considered a complex quantity and is given by the following Equation (3.17):

$$N = n_\circ + ik_\circ \tag{3.17}$$

where N is the complex refractive index, n_0 and k_0 is the real and imaginary part of the refractive index.

Refractive index n_0 for thin films can be determined from Equation (3.18):

$$n_\circ = \sqrt{\frac{4R}{(R-1)^2} - k_\circ^2} - \left(\frac{R+1}{R-1}\right) \tag{3.18}$$

The extinction coefficient (k_o) represents the amount of energy absorbed, or in other words the amount of energy absorbed by the material from the incident photons. The extinction coefficient is related to the absorption coefficient by the following relationship (Saporal and Herman 1995) Equation (3.19):

$$k_o = \frac{\alpha\lambda}{4\pi} \tag{3.19}$$

Another important optical constant is the dielectric constant. When light incident on an absorbing medium, an interaction occurs between the photons of the incident light and the charges of the medium, and accordingly, energy loss occurs as a result of this interaction, and thus the polarization of the charges of that medium occurs. The amount of energy loss is represented by the dielectric constant (Hummel 2001). From a physical

point of view, it represents the response of the electrons of the material to the electromagnetic field falling on it, and it is given by the following relationship in Equation (3.20):

$$\varepsilon = \varepsilon_1 - i\varepsilon_2 \tag{3.20}$$

where ε_1 and ε_2 are the real and imaginary parts of the dielectric constant, respectively.

The dielectric constant is related to the complex refractive index by the following relationship in Equation (3.21):

$$\mathrm{N}^2 = \varepsilon \tag{3.21}$$

By using Equation (3.19), we get Equation (3.22),

$$\varepsilon_1 - i\varepsilon_2 = (n_\circ - ik_\circ)^2 \tag{3.22}$$

From Equation (3.22), the real and imaginary parts of the dielectric constant can be calculated as follows in Equation (3.23, 24):

$$\varepsilon_1 = n_\circ^2 - k_\circ^2 \tag{3.23}$$

$$\varepsilon_2 = 2n_\circ k_\circ \tag{3.24}$$

The electrical properties of semiconductors depend on several factors (such as indecent light, temperature, doping with foreign elements, and applied magnetic field) that determine the nature of electronic transitions. The electrical conductivity of a semiconductor is highly dependent on temperature. The resistance of a semiconductor decreases with increasing temperature. When light incident on the semiconductor material, the electrons transition from the valence band to the conduction band leaving a hole behind, and these generated electrons and holes contribute to the electric conduction in the semiconductor (Yapifanov 1979).

One of the other important properties of semiconductor thin films to be determined is their electrical properties. Among the electrical properties, electrical values such as conductivity, resistivity, carrier density, and mobility should be examined. The electrical conductivity (σ), which is the reciprocal of the resistivity (ρ) and depends on two main factors: the density of the electric charge carriers, and the mobility of these carriers. The total electrical conductivity of the semiconductor is the sum of the conductivity resulting from the negative (electrons) and positive (holes) charge carriers (Jwad 2009, Hummel 2001). The current density in semiconductors results from the sum of the electron's current density and the hole's current density as in the following in Equation (3.25), Equation (3.26):

$$J = J_n + J_p \tag{3.25}$$

$$J = (n_e \mu_n + P_e \mu_p) E \tag{3.26}$$

where J_p and J_n are the current density of electrons and holes, P_e and n_e are the number of electrons and holes, μ_n and μ_p mobility of electrons and holes, E is the strength of the applied electric field.

The Equation (3.27) of the total electrical conductivity is:

$$\sigma = (n_e \mu_n + P_e \mu_p) \tag{3.27}$$

The electrical conductivity Equation with temperature is as in the following Equation (3.28):

$$\sigma_{dc}=\sigma_o \exp\left(\frac{-E_a}{k_B T}\right) \tag{3.28}$$

where $\sigma_{d.c}$ is electrical conductivity, E_a is the activation energy, K_B is Boltzmann's constant (1.38×10^{-23} J/K = 0.086×10^{-3} eV/K), T is absolute temperature (K).

The value of conductivity can be found from the value of the resistance as follows in Equation (3.29), Equation (3.30), and Equation (3.31):

$$\sigma = \frac{1}{\rho} \tag{3.29}$$

$$\rho = R\frac{at}{L} \tag{3.30}$$

$$\rho = R\frac{at}{L} \tag{3.31}$$

where ρ is resistivity, *R* is film resistance, *t* is film thickness, a is electrode width and *L* is the distance between the aluminum electrodes.

3.2 Experimental Details

This chapter describes the types of equipment used in this work and the preparation method of SnO_2, CdS, Cu doped SnO_2 films and SnO_2:Cu/CdS heterostructure and their measurements. Also, a general description is given of the instruments and the measurement techniques used to study the structural, morphological, optical, and electrical properties.

In Figure 3.9, the experimental study of SnO_2, CdS, Cu doped SnO_2 films and SnO_2:Cu/CdS heterostructure, the characterization techniques used, and the schematic diagram of the determined properties are given.

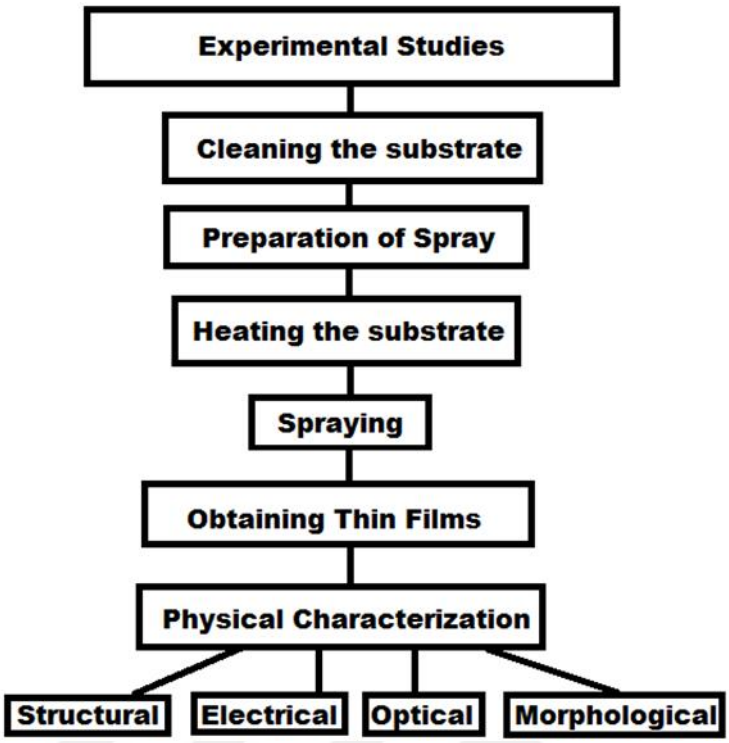

Figure 3.9 A diagram of experimental work of SnO_2, CdS, Cu doped SnO_2 films and SnO_2:Cu/CdS heterostructure

3.2.1 The production of SnO_2:Cu/CdS films by chemical spray pyrolysis

In this thesis, the chemical spraying technique (CSPT) was used for the production of SnO_2, CdS, Cu-doped SnO_2 films, and SnO_2:Cu/CdS heterostructure. The reason for choosing this method is because of its advantages such as low cost, production on different substrates, repeatability, practicality and no need for vacuum.

Figure 3.10 shows the chemical spray pyrolysis set up which consists of the following main parts:

1. Heater
2. Temperature controller
3. Air compressor
4. 100 ml glass container with 1 mm inner diameter nozzle sprayer and inlet for carrier gas.

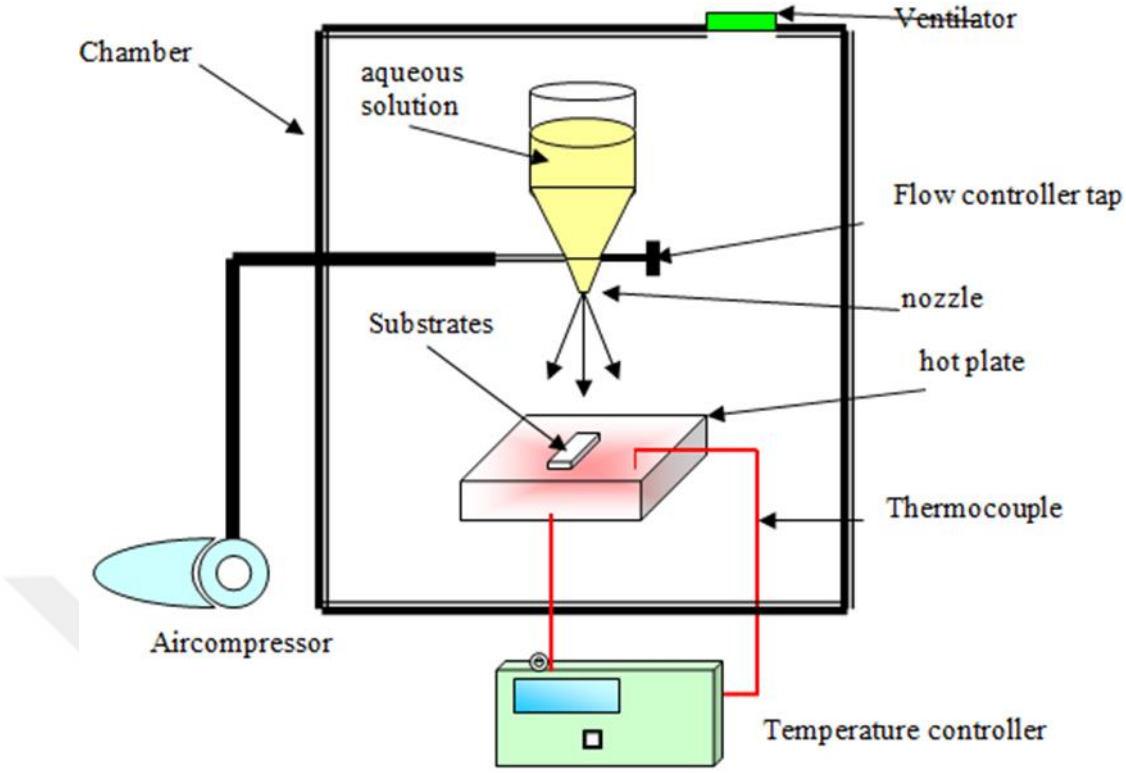

Figure 3.10 Setting of spray pyrolysis equipments (Al-Jabiry 2007)

It is necessary to clean the surface of substrates by using an ultrasound device (Figure 3.11) to remove all grease and dust because the properties of the films (optical, electrical, etc.) are very sensitive to surface preparation. Commercial glass substrates with dimensions (25 × 25 × 1) mm3 were used as substrate.

The process for cleaning the substrates can be summarized in the following steps:

1. Ultrasonically cleaning with distilled water for 10 minute.
2. Ultrasonically cleaning with ethanol for 10 minute.
3. Ultrasonically cleaning with acetone for 10 minute.
4. Drying the substrates using a hot blower.
5. Finally, the weight of the substrate is calculated and then stored in special containers.

Figure 3.11 Ultrasound device

Tin chloride ($SnCl_2{:}2H_2O$) is used as a source of tin ions, copper chloride ($CuCl_2{:}2H_2O$) as a source of copper ions and cadmium chloride ($CdCl_2{:}2H_2O$) as a source of cadmium ions. The mechanism of the film formation is the bonds of tin ions with oxygen ions and then deposited on the substrate

This process depends on the following parameters:

- The molarity of the solutions
- The substrate temperature
- The distance between the substrate and nozzle
- The amount of spray solution
- The carrier gas

All solutions were prepared using the following equationEquation (3.36) is used (AL-Jabiry 2007):

$$M = \frac{W_t}{M_{wt}} \frac{1000}{V} \tag{3.36}$$

where M is molarity, W_t is weight of chemical salt (grams), V is volume of the solution, M_{wt} is molecular weight of chemical salt (grams/moles).

The tin chloride [$SnCl_2{:}2H_2O$], cadmium chloride [$CdCl_2{:}2H_2O$], and copper chloride [$CuCl_2{:}2H_2O$] were used as the solution sources. The molarities of tin chloride, cadminum chloride and copper chloride solutions were adjusted to be 0.02, 0.05 and 0.02 M, respectively. Copper doping was done at the rate of 3 %. All films were produced at a substrate temperature of 350 ºC. The vertial distance between nozel and substrate is 30 cm and sprayin of rate is 2 ml/min.

3.2.2 The determination of thickness of SnO_2:Cu/CdS tilms

The thickness of the prepared film is done by using the sensitive electrical balance of type (Sartorius) with an accuracy of (0.1 mg). The glass substrates are weighed before and after deposition. The thin film thickness is calculated using the following in Equation (3.37) (Chopra 1983):

$$t = \frac{m_2 - m_1}{\rho \times a \times b} \tag{3.37}$$

where m_1 and m_2 are the mass of substrate before and after deposition, a and b are the substrate dimensions, ρ is the density of material, respectivitily. The thickness of the films was determined to be between 250-300 nm.

3.3 Characterization Techniques Used in The Analysis of SnO_2:Cu/CdS Films

The crystal structure of SnO_2:Cu and CdS thin films grown on glass substrates by CSPT was examined by X-ray diffractions using a Philips X-ray diffractometer system. The XRD system recorded the intensity (I) as a function of 2θ over the range of 20º to 60º (Figure 3.12).

The diffraction condition is given by Bragg's law, Equation (3.38):

$$2d_{hkl}\sin(\theta) = n\lambda \tag{3.38}$$

Where d_{hkl} is the distance between the planes (*hkl*) of a crystal lattice, θ is the angle between the incident beam of X-rays and the normal to the plane (*hkl*), *n* is the order of reflection, *n*= 1, 2, 3, ... etc. (Cullity 1978).

The crystallite size (*D*) calculated using the Scherrer formula in Equation (3.39):

$$D = \frac{k\lambda}{\beta\cos\theta} \tag{3.39}$$

where β is the full width at half maximum (FWHM), θ is diffraction angle, *k* is a constant, λ is wavelength (1.54060 Å).

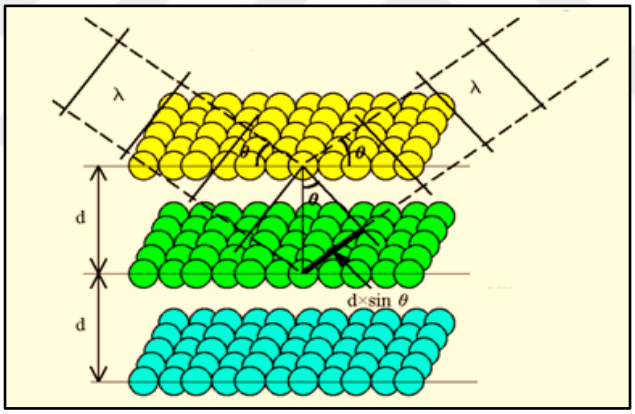

Figure 3.12 Schematic diagram of X-ray diffraction (Cullity 1978)

Atomic force microscopy (AFM) is one of the devices that was used to study the surfaces of pure and copper-doped SnO_2 films deposited on glass substrates. It is used to identify the surface topography, nanosize and surface roughness. It gives a high-resolution two- and three-dimensional image that shows the details of the material surface and roughness. Figure 3.13 shows a simple diagram of an AFM device which consists of a cantilever arm at the end of which is a probe consisting of a sharp tip known as a tip that is used to scan the surface of the sample (Yao Wang 2005).

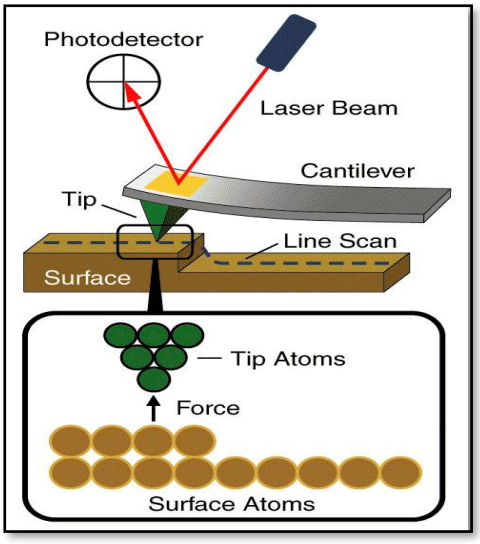

Figure 3.13 The basic concept of AFM (Yao Wang 2005)

A scanning electron microscope (SEM) is a type of electron microscope that produces images of a sample by scanning it with a focused beam of electrons. Electrons interact with atoms in the sample, producing various signals that contain information about the topography and composition of the surface. Electron microscopy (FE-SEM Model Mira3- XMU, TESCAN Japan) was used to obtain the structural parameters such as the size and distribution of the particles through the film surface, as well as the information about the composition of the obtained by the means of EDX measurement.

UV-VIS-Double beam Spectrometer (6800UV/Vis JENWAY) was used to record the optical measurements (Transmittance, Absorbance, and Reflectance) in the wavelength range (300-1100 nm).

The electrical resistivity (ρ) and activation energies (E_a) of the films were determined according to the temperature-dependent conductivity measurement results.

4. RESULT AND DISCUSSION

This chapter includes the results and the analysis of the experimental measurements, which involve the structural, surface, optical, and electrical properties of SnO_2, SnO_2: Cu, CdS, and SnO_2:Cu/CdS films deposited on a glass substrate by CSPT.

4.1 Structural Properties of SnO_2:Cu/CdS Films

Figure 4.1 (a) and (b) show the diffraction pattern of pure copper-doped tin dioxide films deposited on a glass substrate at 350 ºC by CSPT. There are clearly several diffraction peaks of crystalline planes indicating that the crystal structure of the deposited films is a polycrystalline structure. Pure SnO_2 and SnO_2:Cu films possess several crystal planes, which are (110), (101), (200), and (211) at diffraction angles of 26.60, 33.89, 38.03, and 51.82 respectively in the preferred direction (110). There was a decrease in the intensity as a result of doping with copper while the preferred direction did not change. Also, doping with copper led to a decrease in the crystal size calculated from the dominant peak. The parameters obtained from the XRD examinations are represented by the crystal size (D), the distance between the interplanar spacing (d), and the FWHM (β) as shown in Table 4.1. These results are in agreement with the results of researchers (Yao and Wang 2005, Al-Jawad *et al.* 2017).

Figure 4.1 (c) shows X-ray diffraction patterns of CdS prepared at 350 ºC with 0.1 M by CSPT. The crystal structure of the CdS film is a polycrystalline structure with a preferential orientation along (002) direction at $2\theta = 26.60^{o}$. The other peaks were detected at $2\theta = 44$ and 52^{o} which can be ascribed due to reflection from (110), and (112) planes of the hexagonal CdS structure. Figure 4.1 (d) shows the XRD patterns of SnO_2:Cu/CdS films and the prepared film was a polycrystalline structure.

The XRD patterns of the SnO_2:Cu/CdS film are indicative of tetragonal and hexagonal which are attributed to SnO_2 and CdS structure respectively. We note that there is no change in the preferential orientation along (110) direction at $2\theta = 26.6^{o}$ of SnO_2 and

CdS films. The other peaks were detected at 2θ= 33.8, 38, 44, and 52º which can be ascribed due to (101), (200), (110), and (201) reflection planes of the tetragonal SnO_2: Cu/CdS structure, respectively. SnO_2:Cu/CdS films had the highest peak intensity and clearly decreased values in FWHM.

In addition, it was determined that the crystal size of these films was much higher than the other films. Since this would reduce the defects caused by grain boundaries, it also affected other properties of the films, especially their structural properties.

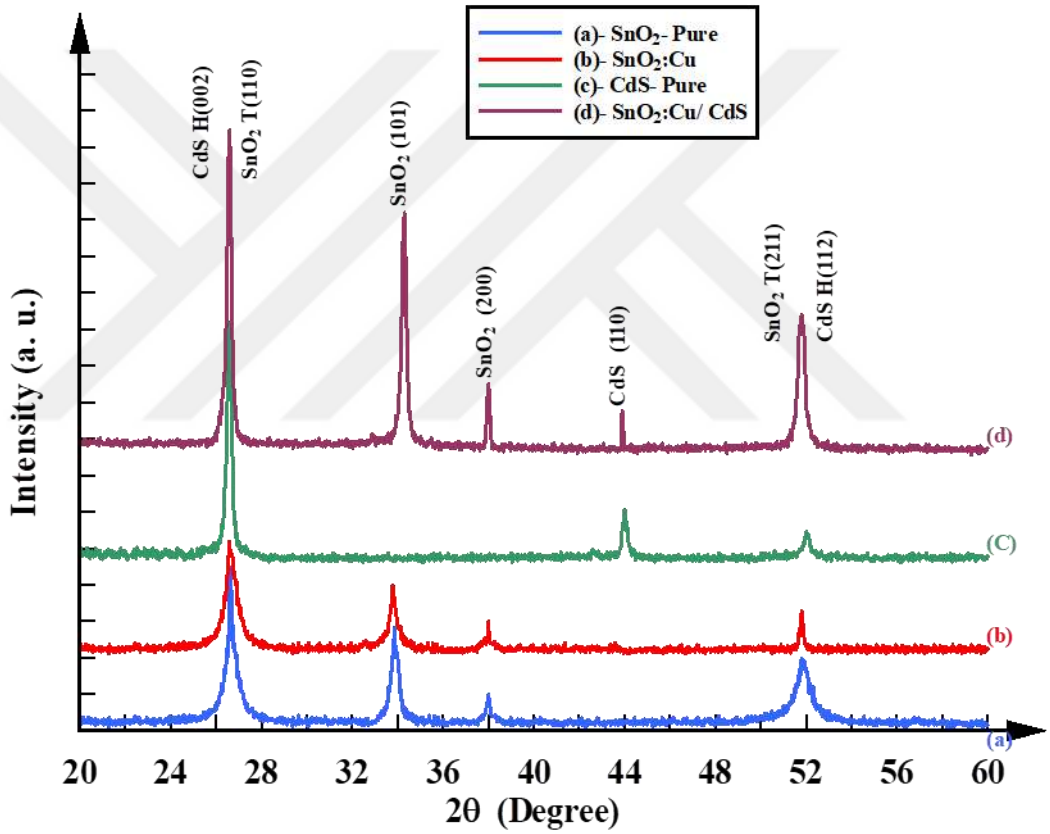

Figure 4.1 X-ray pattern of (a) pure SnO_2, (b) SnO_2: Cu, (c) CdS and (d) SnO_2:Cu/CdS films

Table 4.1 X-ray diffraction results of prepared films

FILMS	2θ (°)	d (Å)	(hkl)	Crystalline Sturucture	D (nm)	$\delta(nm^{-1})^2\times10^{-3}$
SnO_2 pure	26.6	3.3473	(110)	Tetragonal	8	15.6
SnO_2:Cu	26.6	3.3439	(110)	Tetragonal	14.5	4.75
CdS	26.6	3.3360	(002)	Hexagonal	30.5	1.07
SnO_2: Cu/CdS	26.6	3.3698	(110) (002)	Hexagonal Tetragonal	56.04	31.8

4.2 Surface Properties of SnO_2:Cu/CdS Films

The study of the surface of the semiconductor films is of great importance to know its surface topography and roughness. The increase in the surface roughness leads to the scattering of light and thus the loss of an amount of transmitted light. Many applications require a smooth surface (low roughness) as in solar cells because the uneven surface causes disorders in the junction region and reduces efficiency. Atomic force microcope (AFM) results enable us to know a number of parameters such as the surface roughness, the root mean square value of the roughness, and the average grain size.

Figure 4.2 shows two and three-dimensional images of (SnO_2, SnO_2:Cu, CdS, SnO_2:Cu/CdS) films deposited on glass substrates using the CSPT technique. It is clear that the distribution of grains on the surface is almost uniform and homogeneous, and the film is without any cracks. The results showed that the average surface roughness of the SnO_2 film is (10.7 nm), and this value increases to (2.61 nm) when doping the SnO_2 film with copper by 3 %.

Besides, the average grain size of the SnO_2 film decreases from 69.31 nm to 25.04 nm by doping with copper. While the surface roughness of CdS and SnO_2:Cu/CdS films was 17.6 nm and 18.8 nm, respectively. The small surface roughness values indicate an increase in the surface smoothness and these features of the film surfaces enable us to

use these films as a window layer or buffer layer in solar cell applications as well as many other applications. A smoother surface leads to a decrease in reflectivity and an increase in the absorption of electromagnetic energy falling on the film, and this is in agreement with the results of the researchers. Table 4.2 summarizes the results obtained from the atomic force microscopy of the prepared films.

Table 4.2 Atomic force microscopy results for the prepared films

FILMS	ROOT MEAN SQUARE (nm)	ROUGHNESS AVERAGE (nm)	TEN POINT HEIGHT (nm)	AVERAGE GRAIN SIZE (nm)
SnO_2	13.2	10.7	58.3	69.31
SnO_2:Cu	3.08	2.61	7.88	25.04
CdS	21.4	17.6	93.6	85.14
SnO_2:Cu/CdS	22.6	18.8	96	87.13

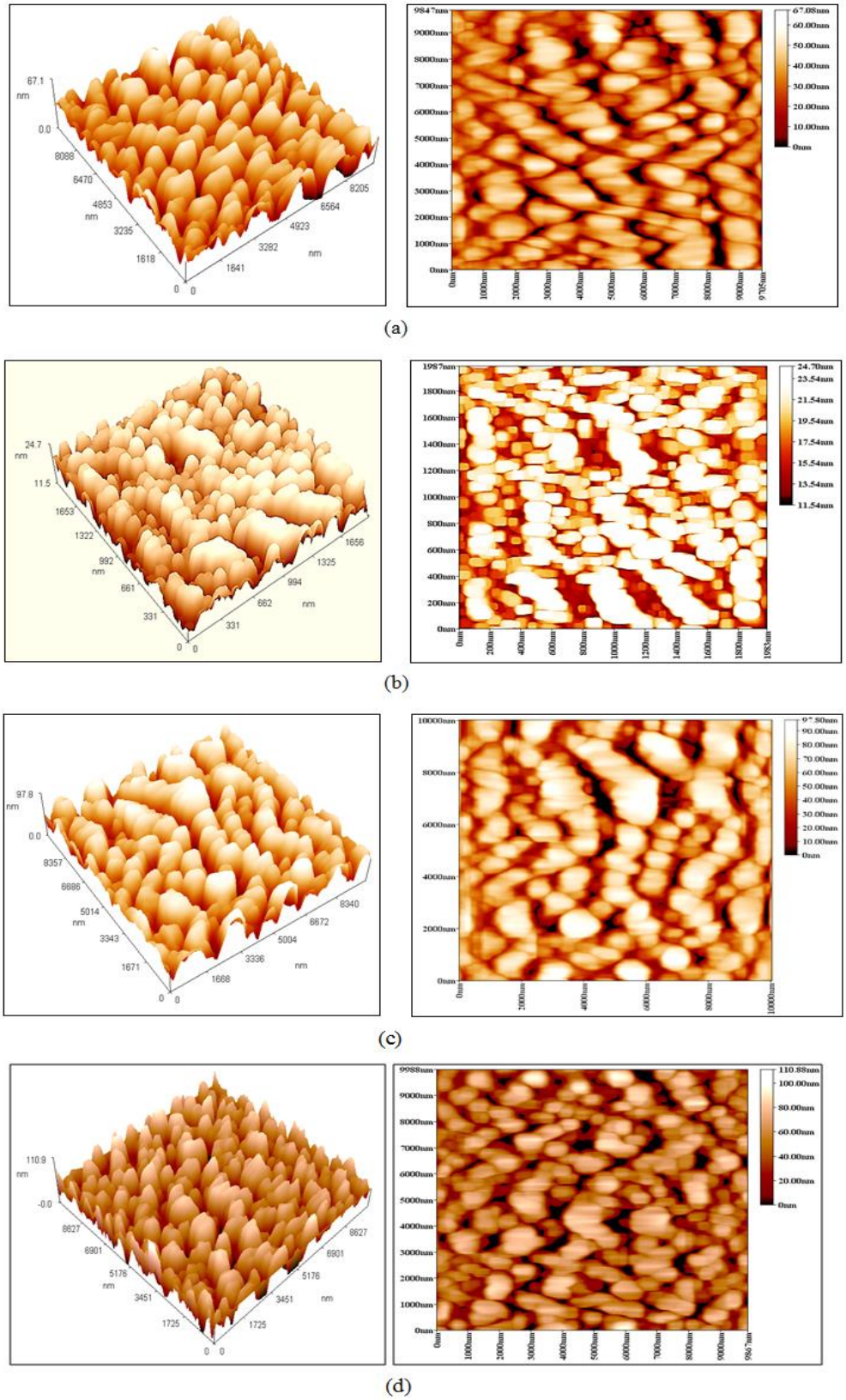

Figure 4.2 AFM images of (a) SnO_2, (b) SnO_2:Cu (c) CdS films and (d) SnO_2:Cu/CdS films

A Scanning Electron Microscope (SEM) was used to examine the surface morphology and to determine the particle size of the films (SnO_2, SnO_2:Cu, CdS, SnO_2:Cu/CdS) Figure 4.3 shows SEM images of these films. It is clear that the surfaces of the prepared films have spherical particles, with a homogeneous distribution on the substrate, and there are no cracks on the surface of the film or large molecular agglomerations. The formation of the film surface depends on the method of preparation and deposition parameters of the (CSPT) system. The surface of the prepared film consists of spherical nanoparticles as well as granules of nanoparticles that gathered as a result of deposition and formed large granules on the surface of the film. The average particle size value of the films (SnO_2, SnO_2:Cu, CdS, SnO_2:Cu/CdS) were 23.224, 23.892, 22.554, and 22.143 nm, respectively. Cu-doped SnO_2 films have better dispersion and homogeneity (Figure. 4.3 (b)). It was determined that the grain sizes determined by SEM analyses were close to each other in all films. Intensive formation of SnO_2 and CdS films occurred on the surface. CdS films have a homogeneous surface consisting of larger particles than SnO_2 films. The grainy structure of the SnO_2 films has become more pronounced with Cu doping.

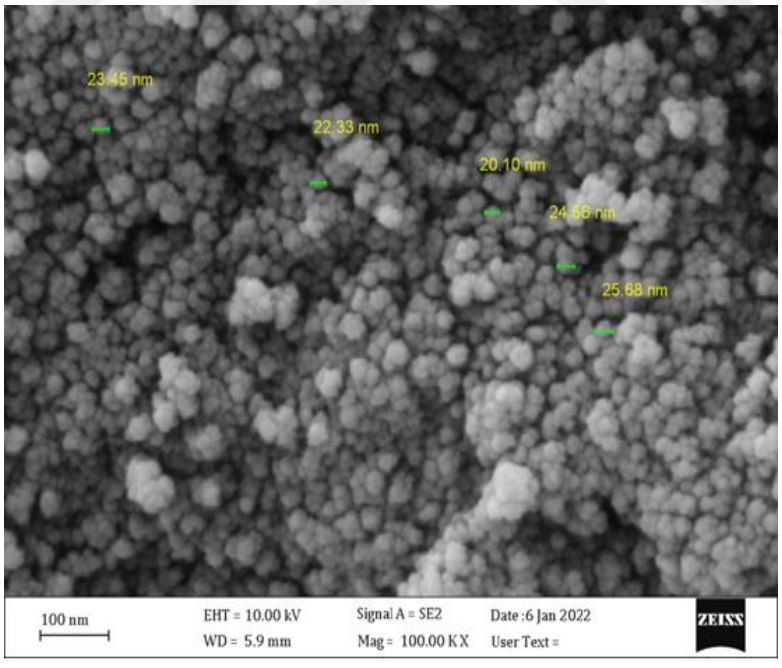

Figure 4.3 (a) SEM image of pure SnO_2

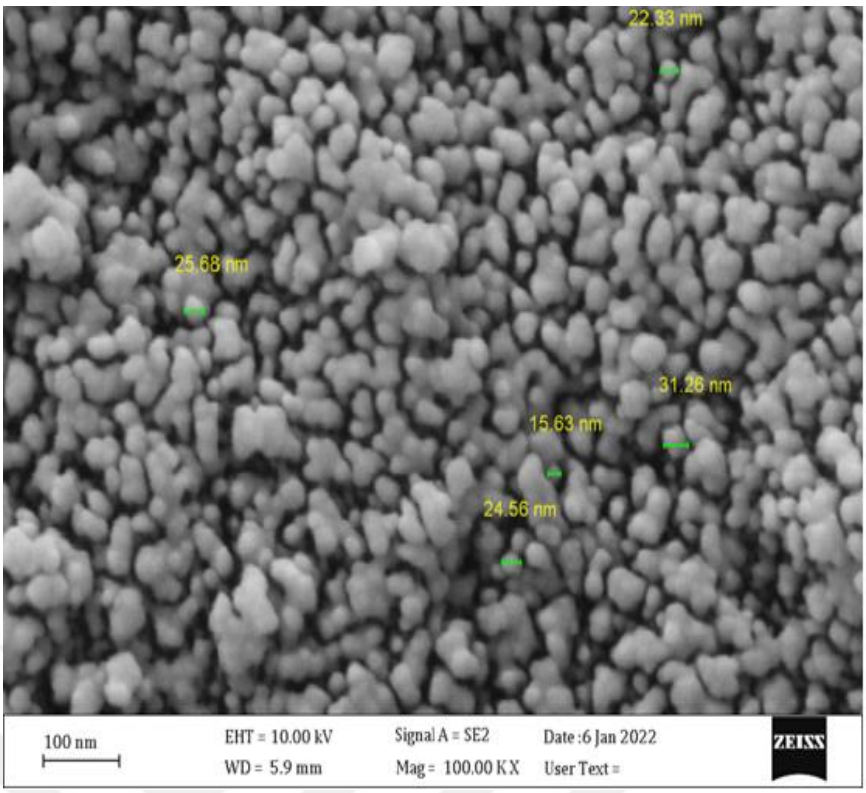

Figure 4.3 (b) SEM image of SnO_2: Cu

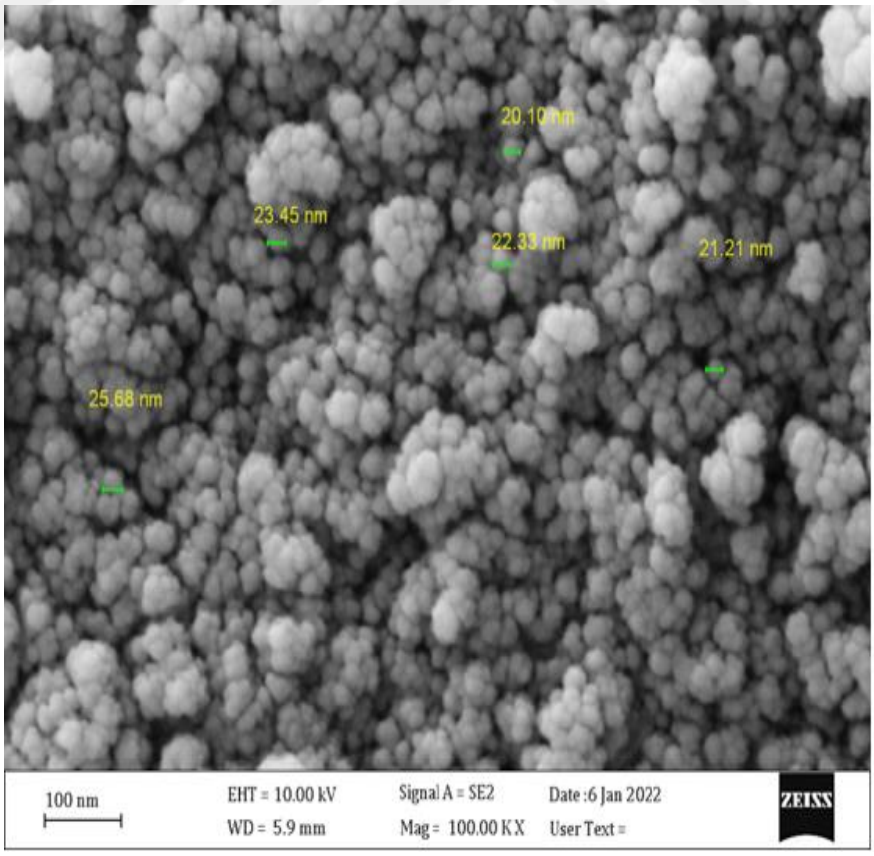

Figure 4.3 (c) SEM image of CdS

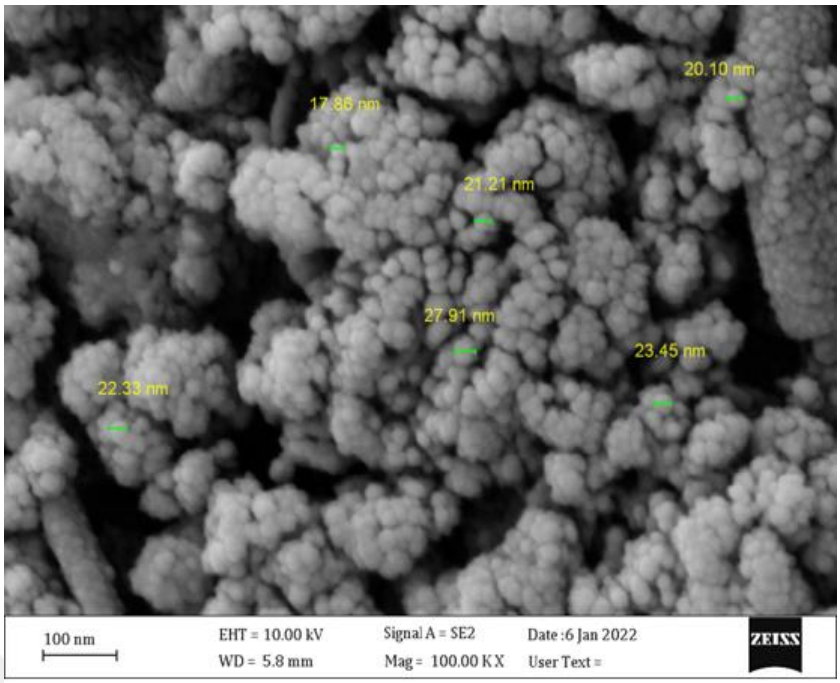

Figure 4.3 (d) SEM image of SnO_2:Cu/CdS films

Energy-dispersive X-ray spectroscopy (EDX) was used to find out the chemical composition and parentage of the elements from which the prepared films were formed. Figure 4.4 shows the elements that formed the film (SnO_2) which are tin (Sn), chlorine (Cl), oxygen (O), and silicon (Si)). In addition, elements obtained from base materials such as si and other elements with the same peak values were observed in the spectra. The ratios of these elements in the structure are given in Table 4.3. The appearance of the element copper in Figure 4.4 is a result of doping a solution of tin chloride (SnCl2.2H2O) with copper chloride ($CuCl_2.2H_2O$) by (3 %). The presence of elements (calcium (Ca), silicon (Si)), chlorine (Cl), and oxygen was also observed. We think that these elements may come from the glass substrate. CdS film is one of the best buffers used in solar cells, so knowing its chemical composition is essential. Figure 4.4, Figure 4.5, Figure 4.6, and Figure 4.7 shows the results of (EDX) for the film (CdS). The following elements (Si, Cl, S, Cd) were observed. EDX results for (SnO_2: Cu/CdS) film are shown in Figure 4.8. We note the presence of elements (Sn, Cd, S, Cl, O, Si, Ca) as well as a small percentage of potassium (K). The element ratios of the prepared films (SnO_2, SnO_2:Cu, CdS, SnO_2:Cu/CdS) are shown in Table 4.3.

Table 4.3 EDX results for the prepared films

FILMS	ELEMENT (Wt %)								
	Sn	**O**	**Cu**	**Si**	**Cd**	**S**	**Cl**	**Ca**	**K**
SnO_2	86.96	9.57	----	2.65	----	----	0.82	----	----
SnO_2:Cu	79.95	11.92	4.75	2.52	----	----	0.54	0.32	----
CdS	----	----	----	2.43	82.64	14.7	0.23	----	----
SnO_2:Cu/CdS	68.73	5.83	----	2.07	19.98	2.99	----	0.21	0.19

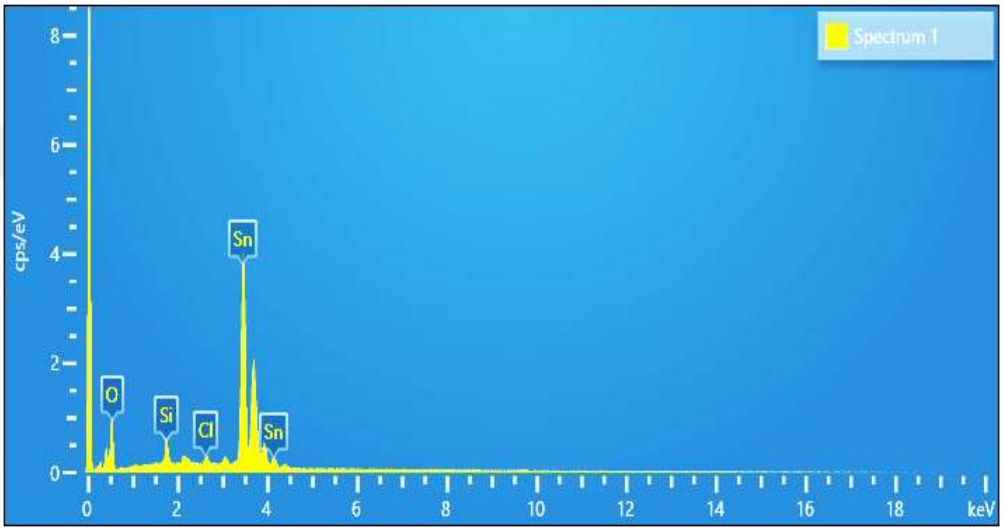

Figure 4.4 EDX image of SnO_2 film

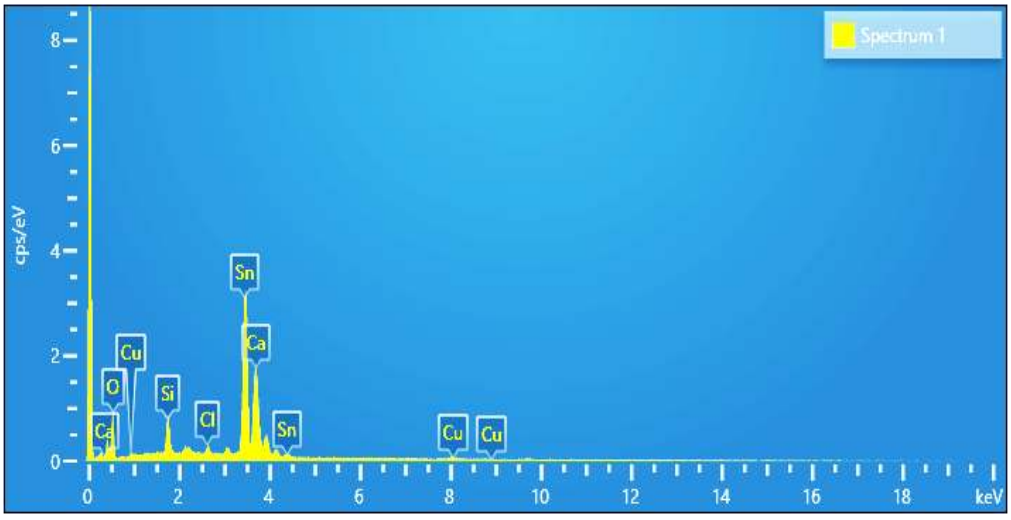

Figure 4.5 EDX image of SnO_2:Cu film

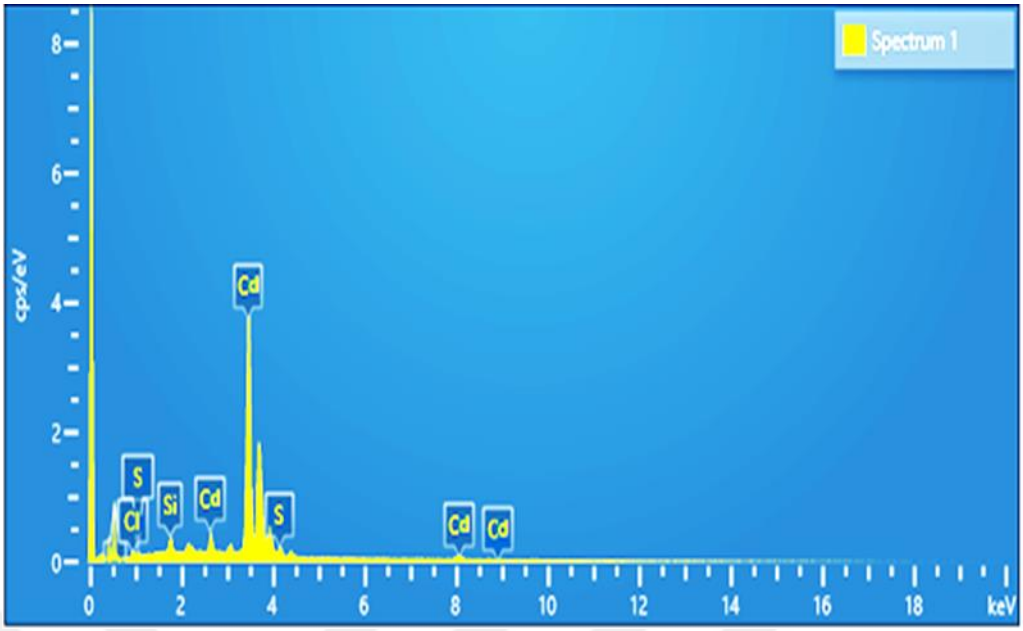

Figure 4.6 EDX image of CdS film

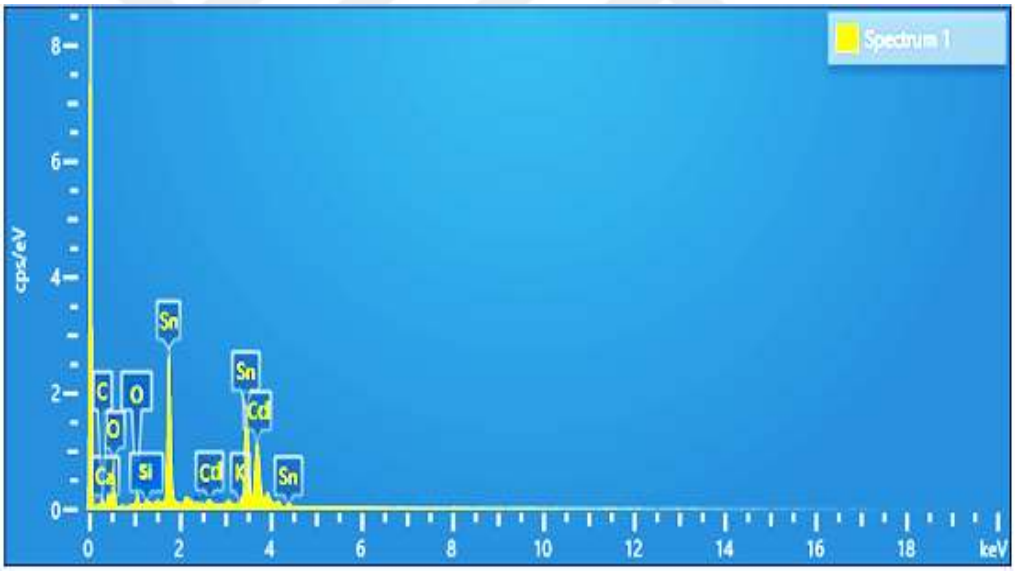

Figure 4.7 EDX image of SnO_2:Cu/CdS film

4.3 Optical Properties of SnO_2:Cu/CdS Films

The transmittance (*T*) is defined as the ratio between the intensity of the transmission radiation and the intensity of the incident radiation on the film. The transmittance depends on the type of material, crystal structure, the thickness of the prepared films,

and the nature of the film surface. Through the transmittance and absorption spectra, we can know the properties of the optical material at different wavelengths.

In addition, two factors affect the transmittance of the prepared films, which are the surface features of the thin films and the thickness of the films. Depending on the transmittance and absorption spectra, we can know the properties of the optical material for different wavelengths, as well as two parameters that affect the transmittance of the prepared films, namely, the surface defects of the film and the roughness of the surface of the film. Figure 4.8, shows the transmittance as a function of wavelength in the range (300-1100) nm for (SnO_2, SnO_2:Cu, CdS, SnO2:Cu/CdS) films prepared by (CSPT). We note that all the prepared films have a high transmittance (greater than 70 %) except CdS and SnO_2:Cu/CdS. Besides, the pure SnO_2 film has the highest transmittance (greater than 84 % at 550 nm), while the SnO_2:Cu/CdS film has a lower transmittance. The SnO_2:Cu/CdS film can be used as a window to solar radiation as well as its use as a window layer in solar cells.

Absorption coefficient (α) as a function of the wavelength of films (SnO_2, SnO_2:Cu, SnO_2:Cu/CdS, and CdS) deposited by pyrolysis method on glass substrates at a temperature of (350 ºC) shown in Figure 4.9. When doping a SnO_2 film with copper (Cu), the absorption coefficient increases due to copper having a high absorption coefficient, which leads to an increase in absorbance and a decrease in transmittance.

In general, all the prepared films have a low absorption coefficient and different values of the absorption coefficient which leads to the difference in the optical path of the rays inside the film. Despite the slight increase in the absorption coefficient of the SnO_2:Cu/CdS film, it can be used as a window and conductive layer in a solar cell.

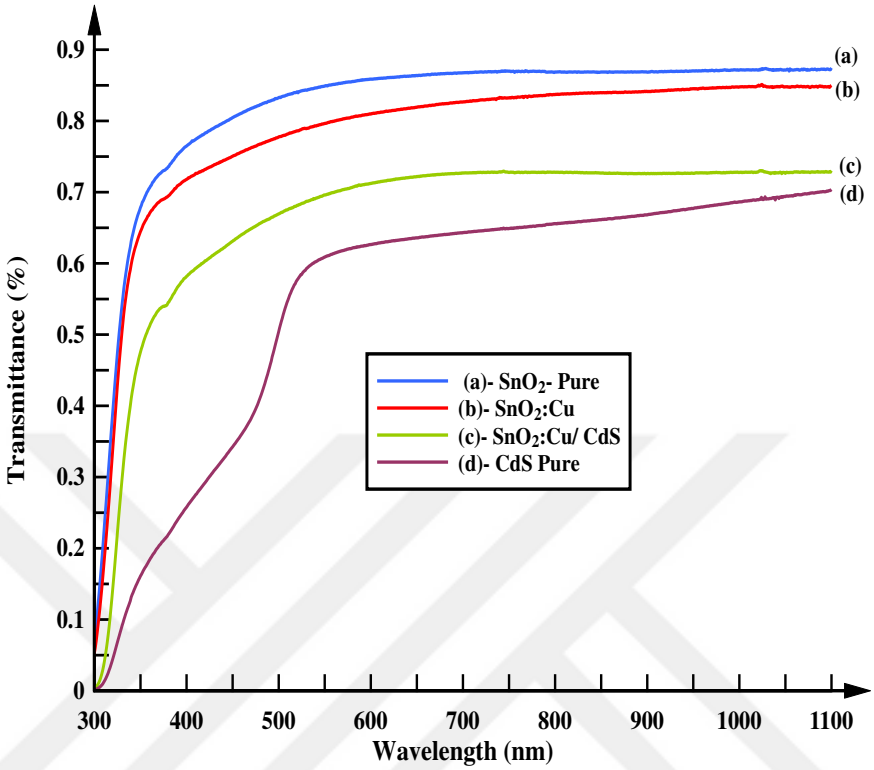

Figure 4.8 Transmittance spectra of SnO_2, SnO_2:Cu, SnO_2:Cu/CdS, and CdS films

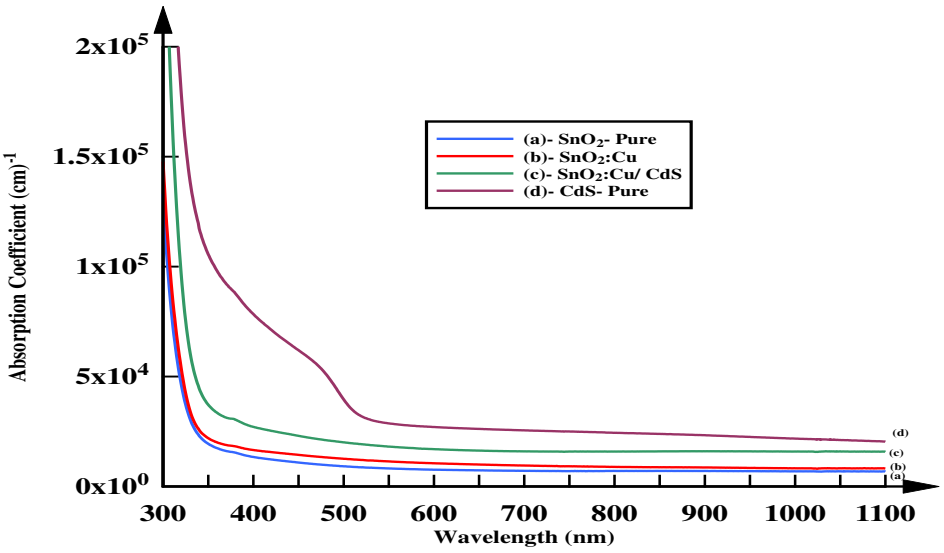

Figure 4.9 Absorption coefficient spectra of SnO_2, SnO_2:Cu, SnO_2:Cu/CdS, and CdS films

The optical energy gap is one of the most important constants in semiconductor physics, enabling the recognition of the suitability of films in various applications such as solar cells, diode emitters, photovoltaic cells, solar detectors and others. The most important factors affecting the energy range are experimental parameters such as the type of material, synthesis method, impurities, deposition temperature and other preparation conditions. The optical band gap energy allowed for direct transitions was calculated by the Tauc model in Equation (2.18) by plotting the graphical relationship between $(\alpha hv)^2$ as a function of photon energy (hv) as shown in Figure 4.10.

The intersection of the straight portion of the curve with the photon energy axis (hv) represents the value of the optical energy gap. The calculated energy gap values for SnO_2, SnO_2:Cu, SnO_2:Cu/CdS, and CdS films were 3.90, 3.88, 3.75 and 2.28 eV respectively. The decrease in the energy gap indicates the creation of new localized levels below the conduction bands and above the valence within the band gap region. Doping of 3% Cu did not cause a significant change in the band gap values of the SnO_2 films. It has been determined that SnO_2:Cu/CdS films have wide band gap value, which is one of the transparent conductive oxide properties. In terms of band gap value, SnO_2:Cu/CdS films are suitable for use in solar cells.

The refractive index (n) is the ratio between the velocities of light in a vacuum to the velocity of a substance. The refractive index depends on many factors, including the type and thickness of the film. The refractive index (n_o) of the thin film is related to the reflectivity (R) and the extinction coefficient (k_o) (Equation 2.22). Figure 4.11 shows the variation of the refractive index versus the wavelength of the films (SnO_2, SnO_2:Cu, CdS, and SnO_2:Cu/CdS). It is clear that the refractive index increases gradually with increasing wavelength, and its value is at the middle of the visible region for the films SnO_2, SnO_2:Cu, CdS, and SnO_2:Cu/CdS, respectively. Besides, the refractive index of SnO_2 thin films increases with Cu doping. The SnO_2:Cu/CdS films have thehighest refrective index values in the visible region. The variation in the refractive index values of the prepared films is attributed to the difference in the density of the materials.

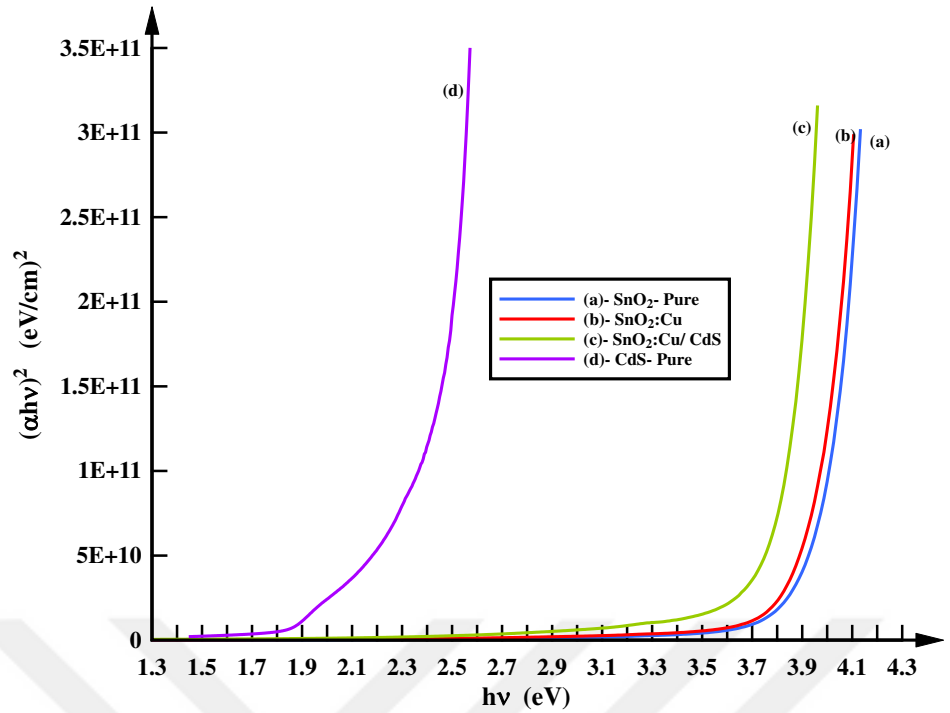

Figure 4.10 Optical energy gap of SnO_2, SnO_2:Cu, SnO_2:Cu/CdS, and CdS films

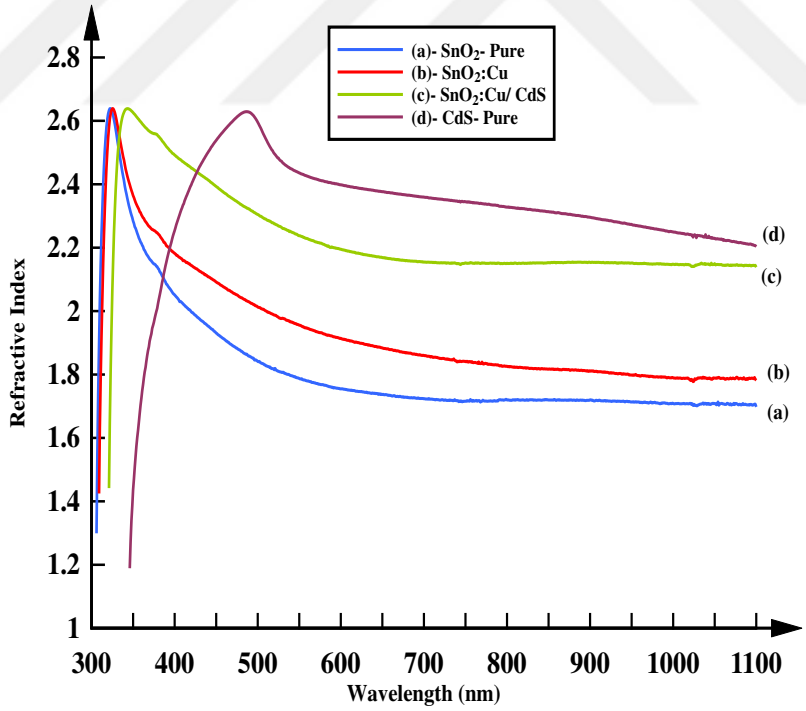

Figure 4.11 Refractive index (n) of SnO_2, SnO_2:Cu, SnO_2:Cu/CdS, and CdS films

The extinction coefficient (k) represents the attenuation of the electromagnetic wave in the film and is the amount of energy of the incident photons absorbed by the electrons of the material. The extinction coefficient was calculated using the absorption coefficient Equation (2.22). Figure 4.12 represents the variation of the extinction parameter with the wavelength of the (SnO_2, SnO_2:Cu, SnO_2:Cu/CdS, and CdS) films prepared at 350 ºC by CSPT. From the observation of the figure, we find that the curves of the extinction coefficient are similar to the curves of the absorption coefficient. The extinction coefficient increases slightly with the increase of the wavelength for all the prepared films. The extinction coefficient decreases rapidly at wavelengths (photonic energies) corresponding to the absorption edge, and this decrease may be due to the significant decrease in the absorption coefficient at these wavelengths. The fall in extinction coefficient may be due to the absorption of light at the grain boundaries. It is almost consistent in the higher wavelength region. The behavior of the extinction coefficient is nearly similar to the corresponding absorption coefficient for SnO2 thin films as reported (Baco *et al.* 2012; Pervas *et al.* 2020).

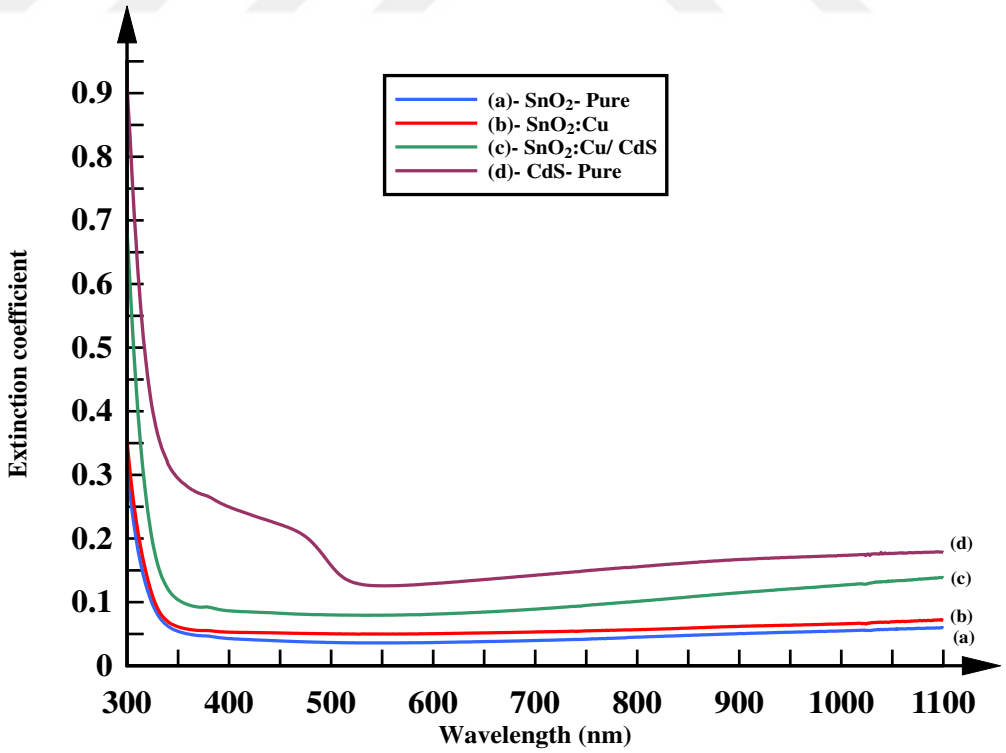

Figure 4.12 Extinction coefficient of SnO_2, SnO_2:Cu, SnO_2:Cu/CdS, and CdS films

4.4 Electrical Properties of SnO_2:Cu/CdS Films

The continuous electrical conductivity ($\sigma_{d.c}$) has been studied depending on the resistance variation with temperature to find the values of activation energy for SnO_2, SnO_2:Cu, SnO_2:Cu/CdS, and CdS films. The value of the film's resistance (R) was recorded for the temperature range. Then the electrical conductivity was calculated. Figure 4.13 and Figure 4.16 shows the relationship between ($ln\sigma$) and ($\frac{10^3}{T}$). The activation energy of the prepared films was calculated using Equation (3.28). Figures 4.13, 4.14, 4.15, and 4.16 results clearly show that the conductivity for all films displays semiconducting behavior. Also, it is clear from the figure that the electrical conductivity increases in an exponential relationship with the increase in temperature.

All temperature range was set apart from two regions. As is known, Sn intertitials and O vacancies lead to a donor effect like SnO films which have n-type electrical conductivity. We also note the presence of two activation energies; see Table 4.4, the first at low temperatures. The conductivity increases slowly at low temperatures. In this region, the increase of conductivity is determined by that of the donor levels below the conduction band, so the increase in conductivity is small. We can say that the conductivity increases prominently with increasing temperature. These regions indicated that the existence of shallow and deep donors traps energy levels below the donor levels.

The doping of SnO_2 with copper (Cu) increased the electrical conductivity. A similar electrical conductivity effect has been observed in the literature (Darenfad *et al.* 2022). The conductivity of the SnO_2:Cu/CdS film is higher than that of the SnO_2 film and the reason for this can be attributed to a decrease in the density of the grain boundaries of the SnO_2:Cu/CdS film. XRD and SEM results support this situation.

Table 4.4 Activation energies of SnO_2:Cu/CdS films

FILM	E_{a1} (eV)	E_{a2} (eV)	ρ (Ω.cm)
SnO_2 pure	0.705	0.215	8.23×10^{-3}
SnO_2:Cu	0.616	0.167	7.74×10^{-3}
CdS	0.537	0.114	4.59×10^{-2}
SnO_2:Cu/ CdS	0.458	0.103	3.25×10^{-3}

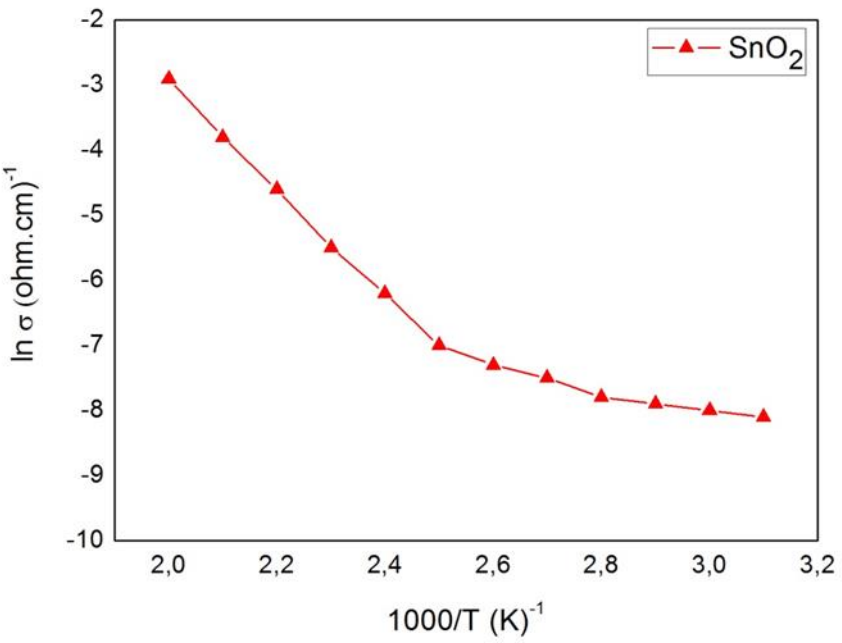

Figure 4.13 Relationship between ($ln\sigma$) and the reciprocal of temperature (1000/T) for (SnO_2) film

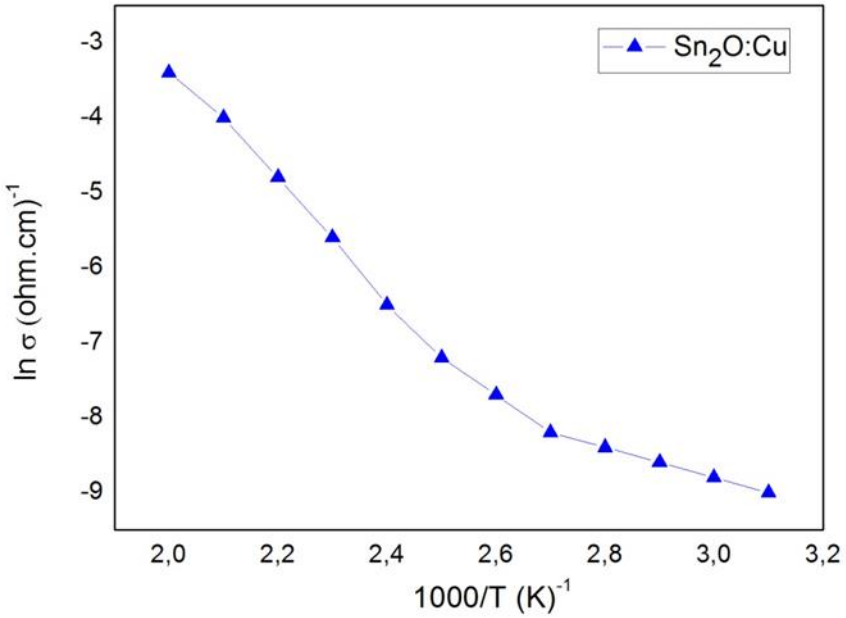

Figure 4.14 Relationship between (*lnσ*) and the reciprocal of temperature (1000/T) for (SnO_2:Cu) film

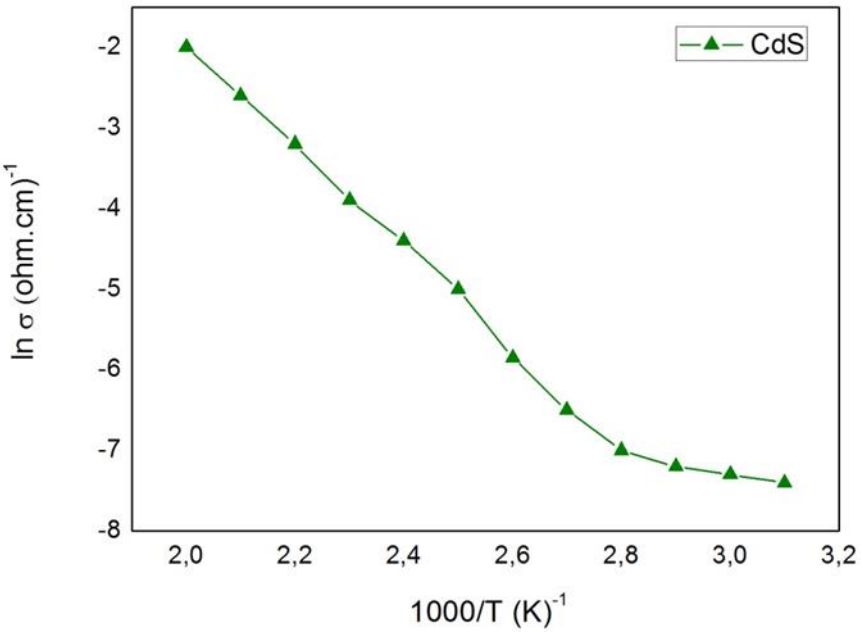

Figure 4.15 Relationship between (*lnσ*) and the reciprocal of temperature (1000/T) for (CdS) film

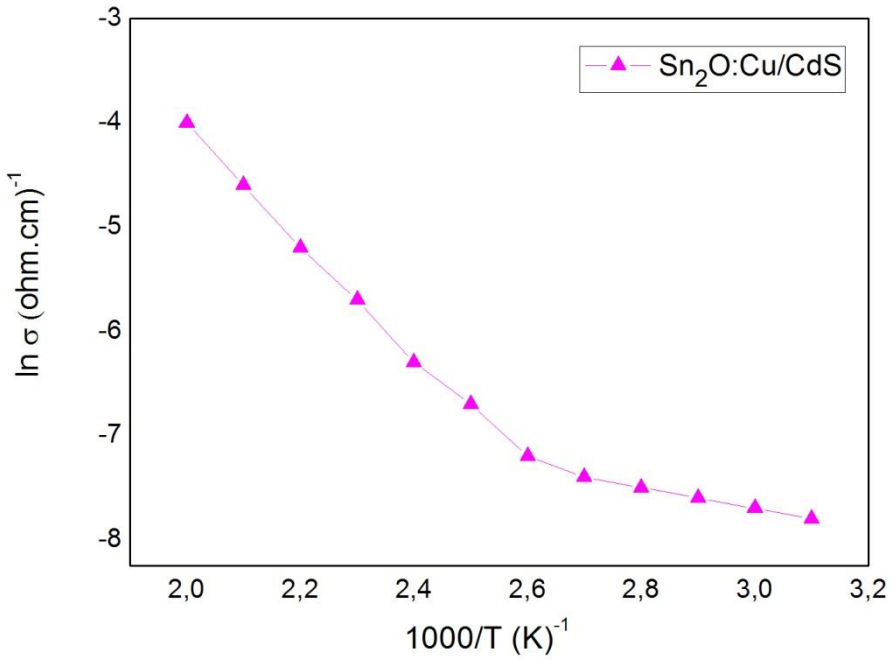

Figure 4.16 Relationship between (*lnσ*) and the reciprocal of temperature (1000/T) for (SnO_2:Cu/CdS) films

5. CONCLUSIONS AND RECOMMENDATION

5.1 Conclusions

In this section, we present the most important conclusions obtained from the current study. Among the films produced, SnO_2:Cu/CdS films have the best crystal structure. These films have the highest peak density, low half-peak width, and large grain size. The roughness values of the SnO_2 films were reduced with the addition of Cu. It was observed that SnO_2:Cu/CdS films had the lowest roughness values. Cu doping increased the grain formation on the surface of the films. The mean grain size was determined as 23 nm. High transmittance (90 %) SnO_2 films were obtained. It was observed that Cu addition reduced the permeability of SnO_2 films. In addition, SnO_2:Cu/CdS films had lower transmittance than other films. The band structure of SnO_2:Cu/CdS films was obtained similar to that of SnO_2 films. The band gap values of SnO_2:Cu/CdS films was calculated as 3.75 eV. The refractive index values of the films in the visible region decreased with the addition of Cu. The mean refractive index of SnO_2:Cu/CdS films was determined to be 2.3. The results of electrical properties showed that the electrical conductivity increased with an exponential relationship with the increase in temperature. All the prepared films have two activation energies and low electrical resistivty value.

5.2 Recommendation

The results of the thesis study are evaluated and different studies that can be done in the future are given below.

A more comprehensive study can be done by using Cu at different doping ratios. The results obtained by doping with different elements such as fluorine and indium can be examined.

The use of different substrates in the production of SnO_2:Cu/CdS films can be examined by varying the experimental parameters such as different substrate temperatures, molarity, solution flow rate, and solution source.

In addition, the effect on the SnO_2:Cu/CdS films can be examined by applying heat treatment applications in different atmospheres after production.

REFERENCES

Abbas, S. I., Hathot, S. F., Abbas, A. S., Salim, A. A. 2021. Influence of Cu doping on structure, morphology and optical characteristics of SnO_2 thin films prepared by chemical bath deposition technique. Optical Materials, 11(7): 111-112.

Abd, A. G. 2012. Studying the structural and optical properties of NiO films. MSc. Thesis, Diyala University, 80 page, Iraq.

Adams, D. R. W. 2007. Nanotechnology Demystified. Rice University. 10(07): 149053.

Al-Dulaimi, R. 2011. Study of the Structural and Optical Properties of $Ni_{(x-1)}$ Zn_xO Films Prepared by Thermochemical Decomposition Method. MSc Thesis, University of Diyala, 105 page, Iraq.

Al-Hakim, R. K. and Hussein, A. X. 1980. Basics of Electronic Engineering. Ministry of Higher Education Press, pp. 3125-3141, Iraq.

Al-Jabiry, A. J. 2007. Studying the Effect of Molarity on the Physical and Sensing Properties of Zinc Oxide Thin Films Prepared by Spray Pyrolysis Technique. applied physics branch, applied sciences department, PhD Thesis, University of Technology, 150 page, Iraq.

Al-Jawad, S. M. H., Elttayf, A. K., Saber, A. S. 2017. Studying structural, optical, electrical, and sensing properties of nanocrystalline SnO_2:Cu films prepared by sol-gel method for CO gas sensor application at low temperature. Surf Rev Lett, 24: 175.

Al-Jubouri, W. F. and Hayati, F. G. 1985. Electrical and Magnetic Properties of Materials. Mosul University Press, 57 page, Iraq.

Baco, S., Chik, A., Yassin, F.M. 2012. Study on optical properties of tin oxide thin film at different annealing temperature. Journal of Science and Technology, 4:1.

Badeker, K. 1907. Electrical conductivity and thermo-electromotive force of some metallic compounds. Ann. Phys, 22: 22.

Bass, M., Stryland, W. V., William, D. R., Wolfe W. L. 1995. Handbook of Optics. Mc Graw-Hill, 1606 page, New York.

Boufaa, N. 2012. Development and characterization of tin oxide nano powders (SnO_2). MSc Thesis, Constantine Mentouri University, 145 page, Algeria.

Chopra, K. L. 1969. Thin Film Phenomena. MC Graw Hill Co., 787 page, New York.

Chopra, K. L. 2005. Thin Film Devices Application. Plenum Press, New York.

Chetri, P., Saikia, B., Choudhury, A. 2013. Structural and optical properties of Cu doped SnO_2 nanoparticles: An experimental and density functional study. J. Appl. Phys., 113: 233514.

Codina, J. M., Steve J. E., Movenza J. F. and Bertpan E. 1984. Electrical properties of ploycrystal line in Doped CdS thin films. J. Appl . Phys., 17: 1679.

Cullity, B. D. 1978. Elements of X-ray Diffraction. AddisonWesley, 531 page, USA.

Darenfad, W., Guermat, N., Mirouh, K. 2022. Analysis of the effect of copper concentration on the structural, morphological, optical and electrical properties of Cu:SnO_2 thin films. 1st International Conference on Engineering and Applied Natural Sciences, May 10-13, 2022, Konya, Turkey, 1-9.

Dekkers, J. M. 2007. Transparent conducting oxides on polymeric substrates by pulsed laser deposition. Ph.D. Thesis, University of Twente, 146 page, Netherlands.

Dolaiet, S., Dey, R., Hussain, S., Bhar, R., Pal, A. K. 2019. Photovoltaic properties of F:SnO_2/CdS/CuO/Ag heterojunction solar cell. Materials Research Bulletin, 109: 1-9.

Eckertova, L. 1977. Physics of Thin Films. Plenum presses, 153 page, New York and London.

Eckertová, L. 1977. Methods of Preparation of Thin Films. Physics of Thin Films, 14: 51.

El-Katori, E. E., Ahmed, M. A., El-Bindary, A. A., Oraby, A. M. 2020. Impact of CdS/SnO_2 heterostructured nanoparticle as visible light active photocatalyst for the removal methylene blue dye. Journal of Photochemistry & Photobiology A: Chemistry, 392: 112.

Gençyılmaz, O. 2013. On the Some Physical Properties of ZnO Films Effect of Co Doping, PhD Thesis, Eskişehir Osmangazi University, 79 page, Turkiye.

Grahn, H. T. 2001. Introduction to semiconductor physics. World scientific publishing, 10 page, London.

Hafdallah, A. 2007. Study of the doping of thin films of ZnO produced by ultrasonic spray, MScThesis, University of Constantine, 125 page, Algeria.

Hamrouni, N. and Balila A. 2017. Structural, optical and electrical study of copper-doped tin oxide strips. MSc. Thesis, 98 page, El Wadi University.

Hasan, M. R., Sayeed, M. A., Hussain, K. M. A. 2020. Effect of Aluminium (Al) and Copper (Cu) Doping on Characteristics of Tin Oxide (SnO_2) Thin Film. IEEE Region 10 Symposium (TENSYMP), 5-7.

Hass, G., Francombe, M. H., Hoffman, R. W. 2013. Physics of thin films: Advances in research and development. Elsevier Publishing, 436 page, London.

Hernández-Arteaga, J. G. R., Moreno-García, H., Rodríguez, A. G., Ali, S. M., Hussain, S. T., Abu Bakar, S., Muhammad, J., Rehman, N. 2021. Effect of doping on the Structural and Optical Properties of SnO, Thin Films fabricated by Aerosol Assisted Chemical Vapor Deposition. Thin Solid Films, 7(24): 138.

Hummel, E. R. 2001. Electronic Properties of Materials. Springer Publishing, 447 page, Belgium.

Ismail, R. M. A. 2008. Enhancement of Photoelectrochemical Characteristics of CdS Thin Film Electrodes Prepared by Chemical Bath Deposition:Effect of Annealing and Rate of Cooling. MSc. Thesis, An-Najah National University, pp. 30-31, Nablus.

Ivashchenko, A. and Kerner, I. 2003. Physical Approches to Improvment of Semiconductors Gas Sensors based on SnO_2 Thin Films. Moldavian J. Phys. Sci., 2: 1-8.

Jagtap, R. and Ambre, A. 2006. Atomic force microscopy (AFM): Basics and its important applications for polymer characterization: An overview. Indian Journal of Engineering and Materials Sciences, 13: 368-384.

Jassem, R. I. 2004. Preparation of CdS:Cu/Si Thermal Light Detector by Chemical Spraying Method. MSc. Thesis, University of Technology, 156 page, Iraq.

Jones, E. W., Barrioz V., Irvine S. J. C., and Lamb D. 2009. Towards ultra-thin CdTe solar cells using MOCVD. Thin Solid Films. 517: 2226-2230.

Jwad, H. 2009. Electronic transport mechanism and optical properties of CdSe junction with different substrates. Ph.D. Thesis , University of Baghdad, 203 page, Baghdad.

Kasap, S. O. 2002. Principle of electronic materials and devices. Mc Graw-Hill Publishing, 252 page, New York.

Khaled, M. B. 2012. Study of Some Optical Properties of Lead Sulfide Films Prepared by Thermochemical Decomposition Method. Journal of Engineering and Technology, 30: 3.

Khlayboonme, S. T. and Thowladda W. 2018. Synthesis and Characterization of Cu-Doped SnO_2 thin Films by Aerosol Pyrolysis Technique for Gas Sensor Application. Key Engineering Materials, 766: 205-210.

King, D. C. and Veal, T. D. 2011. Conductivity in transparent oxide semiconductors. J. Phys. Condens. Matter., 23: 334214.

Kumar, M. 2014. CdS/ SnO_2 Thin Films for Solar Cell Applications. International journal of science and research, 3: 322-323.

Kwok K. N 2002. Complete guide to semiconductor devices. IEEE Press, 431-437.

Leaver, K. D. 1971. Thin Films. Wykeham Publications London (L.T.D), London.

Liu, Y., Zhang, P., Tian, B., Zhang, J. 2015. Core Shell Structural CdS@ SnO_2 Nanorods with Excellent Visible- Light Photocatalytic Activity for the Selective Oxidation of Benzyl Alcohol to Benzaldehyde. ACS Appl. Mater. Interfaces., 7(25): 13849–13858.

Maache, M. 2014. Preparation of thin films of semiconductor oxides by sol-gel route. MSc. Thesis, Mohamed Khider Biskra University, 96 page, Algeria.

Mahdi, A. A. 2016. Preparation of Thin Films from ZrO_2: (Co,Ti) Nano-crystalline by Thermal Chemical Spray Deposition Method and Obtaining a Gas Sensor. MSc. Thesis, Al-Qadisiyah University, 106 page, Iraq.

Mattox, D. and Mattox V. 2007. Review of transparent conductive oxides (TCO), Society of Vacuum Coaters, 1: 1-8.

Millaman, J. 1979. Microelectronics. Murray-Hill Publishing, 172 page, Kogakusha.

Mohammad, J. F. and Mohammed, R. I. 2020. Nanocrystalline SnO_2/TiO_2 for Solar Cells Applications. IOP Conference Series: Materials Science and Engineering, 9(28): 072-073.

Mott, N. F., and Davis E. A. 1979. Electronic Processes in Non-Crystalline Materials. Clarendon Press, 608 page, Oxford.

Neaman, D. A. 1992. Semiconductor Physics and Devices. Basic Principles, Richard D. Irwin, Inc., 302 page, Boston.

Orimi, R. L. and Maghouli M. 2016. Optical characterization of SnO_2 nanostructure thin films, annealed at different temperatures. Optik, 127: 263-266.

Pankove, J. I., 1971. Optical Processes in Semiconductors. Prentice-Hall Publishing, 422 page, New Jersey.

Parves, S., Mina, S., Nahid, F., Hussain, K. M. A., Habib, A. 2020. Optical and Structural Properties of Vacuum Evaporated Tin Oxide (SnO_2) Thin Films. International Research Journal of Engineering and Technology, 7 (10): 2-7.

Paufler, P., Barrett, C. S., Massalski, T.B. 1980. Structure of Metals. Pergamon Press, 982 page, Oxford.

Paufler C. S. Barrett. T. B. Massalski. 1980. Structure of Metals. Pergamon Press Oxford, New York, Toronto, Sydney, Paris Frankfurt/M, ().

Perdnis, D. and Gauckler, L. J. 2005. Thin Film Deposition Using Spray Pyrolysis. Journal of Electroceramics, 14: 103-111.

Postek, M. T., Howard, K. S., Johnson, A. H., McMichael, K. L..1980. Scanning Electron Microscopy: A Student's Handbook. Ladd Research Ind., 352 page, New York.

Ray, B. 1969. II-VI Compounds. Printed in Great Britain, 64 page, London.

Ravindra, N. M., Ganapathy, P., Choi J. 2007. Energy gap–refractive index relations in semiconductors-An overview. Infrared Physics & Technology, 50: 21-29.

Reddy, C. V., Ravikumar, R.V., Srinivas, G., Shim, J., Cho. M. 2017. Structural, optical, and improved photocatalytic properties of CdS/SnO_2 hybrid photocatalyst nanostructure. Materials Science and Engineering B, 22: 63–72.

Rengaraj, S., Hee S., Venkataraj S., Kim Y., Vijayalakshmi S., Repo E., Koistinn A. and Illanpaa M. S., 2011. J. Nanoscience, 11:1-12.

Retnasamy, V., Sauli, Z., Taniselass, S., Ahmad, N., Keng, C. J., Kamarudin, H. 2014. Surface Roughness and Grain Size Analysis of Treated Indium Tin Oxide (ITO) Film. Applied Mechanics and Materials, 680: 131-134.

Robertson, J.1979. Electronic structure of SnO_2, GeO_2, PbO_2, TeO_2 and MgF_2. J. Phys. C Solid State Phys., 12: 4767.

Runyan, W. R. 1975. Semiconductor Measurements and Instrumentation. Mc GRAW-Hill Book company,288 page, New York.

Saleh, J. B. and Labihat S. 2018. Studying the structural and optical properties of nickel oxide (NiO) films doped with copper (CuO). MSc. Thesis, University of Martyr Hama Lakhdar, El Wadi, 102 page, Algeria.

Saporal, B. and Herman, C. 1995. Physics of Semiconductors. Springer Verlag, 998 page, New York.

Seeger, K. 1995. Semiconductor physics: an introduction. Springer Publishing, 293 page, Berlin.

Shaker, D. S., Abass, N. K., Ulwall R. A. 2022. Preparation and study of the Structural, Morphological and Optical properties of pure Tin Oxide Nanoparticle doped with Cu. Baghdad Science Journal, 19: 660-669.

Sharma, R., Kumar, V., Goswami, Y. C. 2021. Excellent flexible Tin Oxide-metal sulfide nanocomposites grown by spin coating chemical route. Chalcogenide Letters, 18: 473-479.

Smith, R. A. 1987. Semiconductors. Cambridge Press, 540 page, London. O.

Stenzel 2005. The Physics of Thin Film Optical Spectra. An Introduction, Winzerlaer Str. 10 , 07745 Jena , Germany.

Su, M., Feng, Z., Feng, Z., Chen, H., Liu, X., Wen, J., Liu, H. 2021. Efficient SnO_2/CdS double electron transport layer for Sb2S3 film solar cell. Journal of Alloys and Compounds, 882: 160707.

Šutta, P. and Jackuliak Q. 1998. X-ray diffraction line profile analysis of strongly textured thin films. Mater. Struct., 5(1): 1-5.

Sze, S. M. 1986. Physics of Semiconductor Devices. John Wily & Sons, 574 page, New York.

Tauc, J. 1974. Amorphous and Liquid Semiconductors. Plenum Press, 545 page, London.

Thompson, B. J. 1964. Optical Science and Engineering. PhD Thesis, University of Rochester, 654 page, New York.

Wang, C. 2009. Multiscale modeling and simulation of Nanocrystalline zirconium oxide. Ph.D. Thesis, University of Nebraskal, 326 page, Lincoln.

Yao Wang, Z. L. 2005. Handbook of Microscopy for Nanotechnology. Spinger Publishing, 751 page, Berlin.

Yahiaoui, S. 2014. The effect of the molarity of the different sources of tin on the properties of the thin films of tin oxide SnO_2 produced by Ultrasonic Spray. MSc. Thesis, Mohamed Khider Biskra University, Algeria.

Yapifanov, G. I. 1979. Introduction to solid state electrons. Physics Todays, 4(12): 68, New Jersey.

Ynineb, F. 2010. Contribution to the development of thin layers of transparent conductive oxides (TCO). MSc. Thesis, 85 page, Deconstantine University. Algeria.

Zhou, X., Mu, Y., Zhang, S., Gao, L., Chen, H., Mu, J., Zhang, X., Zhang, M., Liu, W. 2019. CdS nanoparticles sensitized high energy facets exposed SnO_2 elongated octahedral nanoparticles film for photocatalytic application. Materials Research Bulletin, 111: 118–125.